Lund University

Master's thesis

Method for coupling modulated scattered light from free flying insects to harmonics and their relative phases

Ludvig Anderberg
Martin Patricks

February 28, 2020

Abstract

Using laser it is possible to measure the backscattered light from insects. The resulting signal can then be analysed in order to potentially determine the species of the insect. Estimating the fundamental wing beat frequency (FWBF) of insects is important in order do this classification of species, which is an area of research that has been explored previously. In this thesis, the relative phase of the FWBF and its overtones are analyzed with the matched phase reassignment (MPR) method. The frequencies are estimated with the matched reassignment (MR) method. The results of the phase estimations are dependent on variables such as the FWBF, noise levels and number of overtones. Furthermore, the results from the frequency estimation affects the outcome of the phase estimation to a large extent, making the phase estimations vulnerable to wrongly classified frequencies.

In order to obtain real data an test chamber setup was built with the purpose of producing modulated scattered light from free flying insects. The setup used two continuous-wave lasers with the wavelengths 808 nm and 1320 nm. The setup also used a camera to allow a 3D reconstruction of the recorded insects flight path. This setup worked as intended and recorded data was obtained from fruit flies (*drosophila melanogaster*).

It can be concluded that the phase estimations work well for data with low amounts of noise and for FWBFs. Higher levels of noise corrupt the signal too much for the MPR method to work as intended. The same goes for higher FWBFs where the results are not as good on lower frequencies. This, however, is because of the frequencies being wrongly estimated which in turn leads to incorrect phases.

Keywords: frequency estimation, phase estimation, matched phase reassignment, entomological lidar, modulation spectroscopy, scattered light.

Acknowledgements

We want to thank Prof. Maria Sandsten, Dept. Mathematical Statistics, Lund University for important guidance and help throughout the thesis.

We would also like to thank Assoc. Prof. Mikkel Brydegaard, Samuel Jansson and Meng Li, Dept. Combustion Physics, Lund University for valuable inputs as well as providing data from previous test chambers. Lastly we would like to thank Jessica Abbott, Dept. of Biology, div. evolutionary ecology, for providing us with fruit flies on which we could perform experiments.

Contents

Chapter 1

Introduction

1.1 Background

Insects are crucial components of many ecosystems. The roles they play are many, including spreading seeds for further growth of plants, pollination and being a food source for other animals, all important to keep the circle of life intact [1]. However, some insects pose a threat to humans. Vector-borne diseases are a big challenge to the global public health, where malaria in particular, carried by the anophelines, claims over 400,000 human lives per year [2].

Ways of monitoring and recording insects have been developed before, with the purpose of gaining more information about insects which potentially can be a step in the process of controlling diseases spread by the insects. Using entomological lidar has proven to be very useful as a way to record insects over large distances. However due to the classification of insects being largely dependent on the fundamental wing beat frequency this results in a great difficulty to distinguish insects with very similar wing beat frequency. By investigating the phases between the fundamental wing beat frequency and its overtones more information from the observations could be uncovered. This information is currently discarded but through studying the phases there is hope that the classification will be easier [3],[4]. The task of estimating phases of a signal is not easy. An algorithm for this purpose has been developed, called the matched phase reassignment [5], by Maria Sandsten et al., which will be used in this thesis.

1.2 Recorded insects

Using an entomological lidar large areas can be surveilled with high temporal resolution with relative ease compared to other methods such as pheromone- and sweep net traps [6]. The basic principle behind the lidar is using photodiodes connected to telescope and using the telescope to overlap it with a laser beam both being terminated in a dark cavity. The volume where the laser beam and the field of view of the photodiodes overlap give rise to the probe volume [7]. This volume is where any entering insect can be recorded by the photodiodes. The amount of backscattered light will increase when an object intersects the probe volume. However, in order to

interpret the results from a lidar recording, tests must be done on insects in a closed environment where one can control which insects are being recorded. It is therefore important to build an test chamber setup for controlled measurements on specific species of insects.

A signal recorded with an test chamber setup has the general appearance seen in fig. 1.1:

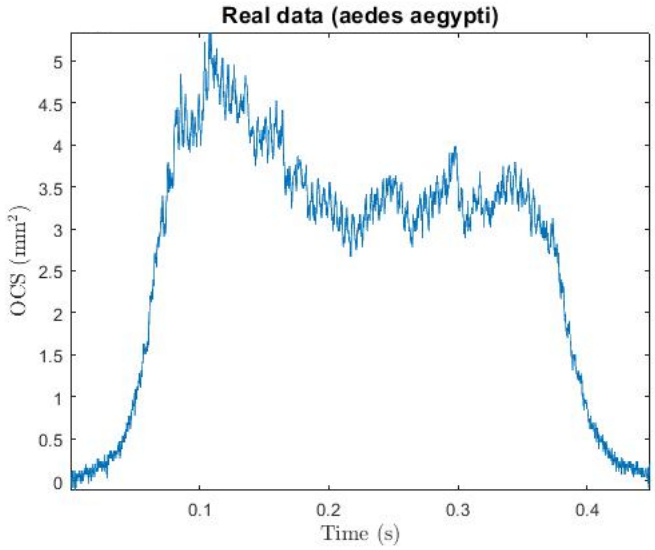

Figure 1.1: Plot of real data, that is to say data acquired through a test chamber, of yellow fever mosquito (*aedes aegypti*) with the optical cross section (OCS) measured in mm^2.

As can be seen in fig. 1.1, the signal has a low-frequency envelope corresponding to the body part of the insect. This is due to the insect's flight path, moving within the laser beam, thus creating a varying intensity. On top of this envelope, the insect's more detailed behaviour can be seen, corresponding to the wing beats that the insect produce in order to fly. These wing beats are fast in comparison to the slow envelope of the body, with a low amplitude in comparison to the low frequency envelope. The commonly used unit in entomological lidar is **O**ptical **C**ross **S**ection (OCS) which is unit describing the optical flux and is usually defined by dropping small teflon balls with a know diameter through the probe volume.

1.2.1 Fundamental wing beat frequency

Previous work on analyzing the frequencies of the insect's wings has been done, see for example [8]. Different species often have different fundamental wing beat frequency (FWBF), which is the frequency of which the insect's wings flap. For example, a male yellow fever mosquito (*aedes aegypti)* has a FWBF of about 889 Hz, variance 57.9 Hz [4], meaning that the insect flaps its wings about 889 times per second. In comparison, the insect commonly known as fruit fly (*drosophila*

melanogaster) has a FWBF of about 202 Hz [8]. It is clear that the FWBF is of great importance when analyzing insects, especially classifying species.

1.2.2 Overtones

The FWBF of an insect can be used to classify the species. However, with the large number of different species of insects, the FWBF is not unique for each species that exist. In addition to the FWBF the recorded signal can also have overtones, also known as harmonics [9]. An overtone is a multiple of the fundamental frequency f_0, i.e. $f = 2nf_0,\ n = 1, 2, 3, ...$ When plotting the spectrum of the signal, these overtones can be seen, illustrated in fig. 1.2:

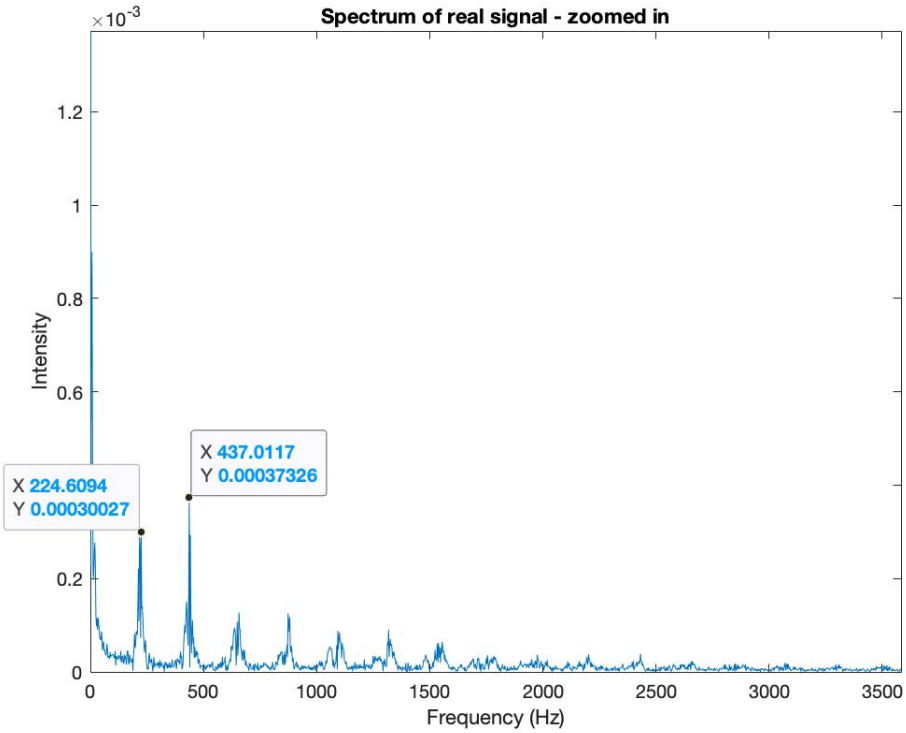

Figure 1.2: Spectrum of the frequency components in the frequency domain from a fruit fly (*drosophila melanogaster).*

As can be seen in fig. 1.2, a multiple of the FWBF of ca 864.5 Hz is present (1729 Hz). Furthermore, in the lower end of the frequencies, the body envelope can be seen. Noise is also present in this signal. This is for illustrative purposes and the theory behind the spectrum will be introduced later on.

1.3 Aim of thesis

This thesis has two main scopes:

1. Estimate the relative phase differences between the fundamental frequency and

its overtones in recorded signals. This will be done by estimating the frequencies of the insect using the matched reassignment method, and from there apply the matched phase reassignment method. If a successful estimation of these phases can be achieved, species-specific phase information might be uncovered.

2. Setting up an "easy-to-use" test chamber setup where it is possible to record live insects with laser as well as recording the insects with a camera. The images from the camera will then be used for 3D reconstruction of the insects flight path.

Chapter 2

Theory

2.1 Phase and periodicity

Define two general oscillating signals,

$$x_1(t) = A_1 \cos(2\pi(f_1 t + \phi_1)) \tag{2.1}$$

$$x_2(t) = A_2 \cos(2\pi(f_2 t + \phi_2)). \tag{2.2}$$

Here, A_1 and A_2 are the amplitudes of the two signals, f_1 and f_2 are the frequencies, and ϕ_1 and ϕ_2 are the two phases. The phases are periodic within the range $[0, 2\pi]$, and for clarity 2π has been factored out to let the phases be within the interval $[0, 1]$. This will also be the case throughout the thesis, the estimated phases will lie in the interval $[0, 1]$, and have the unit 2π radians. The relation between x_1 and x_2 is heavily dependent on frequency and phase. If the frequencies are the same, i.e. $f_1 = f_2$, then the signals will oscillate with the same speed. If also the amplitudes are the same, the signals will thus vary with same speed and have the same height. The last part of the relation between the signals is the phase. If the phases are the same, the two signals will be identical (provided same frequencies and same amplitude). Furthermore, if $\phi_1 = 0$ and $\phi_2 = 1$, the signals will also be identical since 0 and 1 is the range within the phase is periodic. If the phase relation is $\frac{1}{2}$, the signals will look as in fig. 2.1:

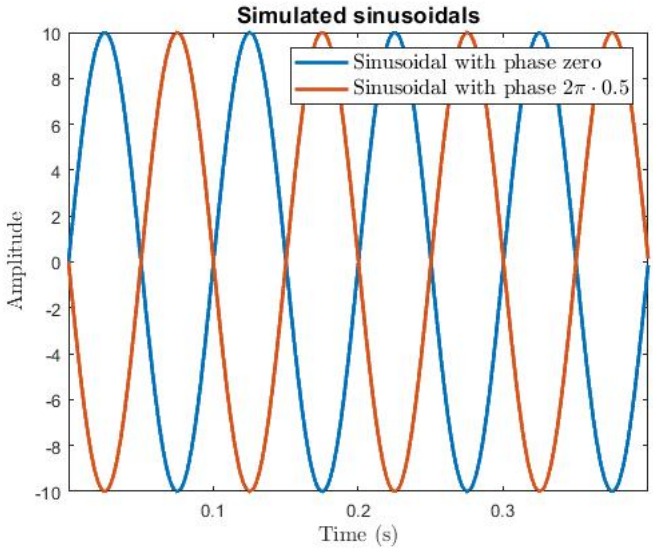

Figure 2.1: Two simulated sinusoidal signals with identical frequencies and amplitudes but different phases.

As can be seen in fig. 2.1, the signals are now completely out of sync. If they were to be summed, they would cancel out each other completely. This is a very different situation than if the phases were to be the same, summation would then provide a signal with twice the intensity instead of total cancellation. In order to illustrate this further, two simulated signals can be seen in fig. 2.2, with their respective spectrums as well.

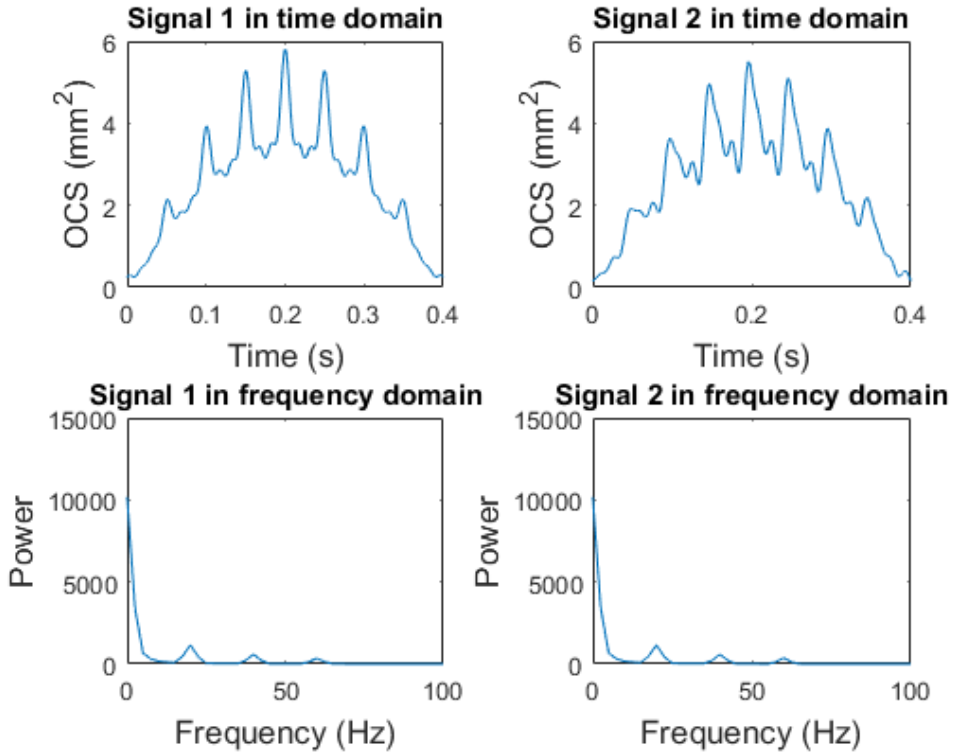

Figure 2.2: Two simulated signals with identical frequencies but different phases shown in both time domain and frequency domain. Simulated with an optical cross section (OCS) in mm^2. In signal 1 all cosines are in phase whereas in signal 2 the phases are $2\pi * 0.1$ and $2\pi * 0.4$

The signals consist of a sum of cosines with varying frequencies, where the only differences between the two signals are the phases. In the time domain, the two signals are visually different and it is not a hard task to tell them apart. Looking at the spectrum though, they seem to be identical. The point is that methods for estimating frequencies only tell a part of the whole story and a lot of information is hidden within the phases.

2.2 Fourier transform and power spectrum

In order to transform a signal to the frequency domain, the Fourier transform can be used, defined as [10]

$$X(\omega) = \int_{-\infty}^{\infty} x(t)e^{-i\omega t}dt. \tag{2.3}$$

Here, $x(t)$ is a continuous and integrable signal. In order to display the power distribution into frequency components, the power spectrum, defined as

$$S_x(\omega) = |X(\omega)|^2 \tag{2.4}$$

can be used.

2.3 Short-time Fourier transform and spectrogram

The Short-Time Fourier Transform (STFT) is a Fourier-transform where the time-domain is included. This has the advantage of instead only displaying the power spectrum, the spectrogram can be calculated. The spectrogram shows the distribution of power in frequency compoenents, over time. It is advantegous to use this when the frequency varies throughout the signal, and is the foundation of the method matched reassignment, which will be introduced in the following section. In order to calculate the STFT, a window $h(t)$, centered at time t is added in the calculation of the Fourier transform of the signal $x(t)$, [10]

$$F_x^h(t,\omega) = \int_{-\infty}^{\infty} x(s)h^*(s-t)e^{-i\omega s}ds. \tag{2.5}$$

A spectrogram is much like the spectrum, but it depicts the frequency content of a signal over time, with a heat map indicating the intensity of the frequency. The spectrum and spectrogram are closely related. If the spectrum was to be taken of a signal in small chunks in time, this would essentially be a spectrogram, although depicted different in the sense it would not have a heat map. The spectrogram is defined as

$$S_x^h(t,\omega) = |F_x^h(t,\omega)|^2. \tag{2.6}$$

The selection of window $h(t)$ affects the behaviour of the spectrogram. The spectrogram cannot have good resolution both in time and frequency which implies a trade-off between the two. Therefore, the choice of window $h(t)$ is important since it directly affects the resolution. A wide window will have a high frequency resolution but low time resolution. This trade-off can be improved by the use of the matched reassignment method, which will be introduced next.

2.4 Matched reassignment

Reassignment is a method that can be used to improve the resolution of the spectrogram by reassigning energy to the local center of gravity. The reassigned spectrogram relocates each value of the spectrogram to the reassignment coordinates, $\hat{t}_x$ and $\hat{\omega}_x$. In the following derviation, all integrals run from $-\infty$ to ∞.

For a signal $x(t) = a(t-t_0)e^{-i\omega_0 t}$, the reassigned spectrogram, with its values relocated to the corresponding reassignment coordinates $\hat{t}_x$ and $\hat{\omega}_x$ is defined as [5]

$$RS_x^h(t,\omega) = \int\int S_x^h(s,\xi)\delta(t-\hat{t}_x(s,\xi),\omega-\hat{\omega}_x(s,\xi))ds\frac{d\xi}{2\pi}, \tag{2.7}$$

with $\int\int f(t,\omega)\delta(t-t_0,\omega-\omega_0)dtd\omega/2\pi = f(t_0,\omega_0)$. For the matched window case, $h(t) = a(-t)$, i.e. a flipped window of the signal, the reassignment vectors are computed as

$$\hat{t}_x(t,\omega) = t + c_1\Re\Big(\frac{F_x^{th}(t,\omega)}{F_x^h(t,\omega)}\Big) = t - c_t\frac{t}{2}, \tag{2.8}$$

$$\hat{\omega}_x(t,\omega) = \omega - c_\omega \Im\Big(\frac{F_x^{\frac{dh}{dt}}(t,\omega)}{F_x^h(t,\omega)}\Big) = \omega - c_\omega \frac{\omega}{2}. \tag{2.9}$$

Here, $\Re$ and $\Im$ represents real and imaginary parts, $F_x^{th}(t,\omega), F_x^{\frac{dh}{dt}}(t,\omega)$ are the STFTs of the signal $x(t)$, with $t \cdot h(t)$ and $dh(t)/dt$ as window functions. The scaled reassignment, $c_t = c_\omega = 2$, reassigns all energy to $\hat{t}_x(t,\omega) = 0, (t_0)$ and $\hat{\omega}_x(t,\omega) = 0, (\omega_0)$.

It is this theory that is the foundation of the matched phase reassignment method, that is to be introduced in the following section.

2.5 Matched phase reassignment

The matched phase reassignment is a method for estimating the phases of a signal, more precisely the phase synchronization of two oscillating transient signals, developed by Maria Sandsten et al. [5]. It is based on the reassigned cross-spectrogram, and it has been shown that the method gives perfect time-frequency localization. As discussed previously, this is the foundation of this thesis. The scope is by using this algorithm estimating the phases of recorded insect signals. As this method is based on synchronization between two signals, surrogate data will be created. This surrogate data, with known phase, will thus be one of the two signals that the synchronization is measured between. The other signal will be real data. Define oscillating signals as

$$y_n(t) = A_n x(t) e^{-i\phi_n}, \quad n = 1, 2. \tag{2.10}$$

where $x(t) = a(t-t_0)e^{-i\omega_0 t}$. For these two signals, the corresponding cross-spectrogram is

$$S^h_{y_1,y_2}(t,\omega) = F^h_{y_1}(t,\omega)(F^h_{y_2}(t,\omega))^*. \tag{2.11}$$

The reassigned cross-spectrum is found by replacing $S^h_x(t,\omega)$ with the absolute value $|S^h_{y_1,y_2}(t,\omega)|$ in the following equation

$$RS^h_x(t,\omega) = \int\int S^h_x(s,\xi)\delta(t - \hat{t}_x(s,\xi), \omega - \hat{\omega}_x(s,\xi))ds\frac{d\xi}{2\pi}. \tag{2.12}$$

Using the following STFTs, expressed for a general signal $y_n(t)$, the reassignment vectors $\hat{t}_{y_1,y_2}(t,\omega)$ and $\hat{\omega}_{y_1,y_2}$ are calculated,

$$\begin{aligned} F^h_{y_n} &= A_n e^{-i\phi_n} F^h_x, \\ F^{th}_{y_n} &= A_n e^{-i\phi_n} F^{th}_x, \\ F^{\frac{dh}{dt}}_{y_n} &= A_n e^{-i\phi_n} F^{\frac{dh}{dt}}_x. \end{aligned} \tag{2.13}$$

The reassignment vectors are then expressed as,

$$\hat{t}_{y_1,y_2} = t + c_t \Re\Big(\frac{F^{th}_{y_1}}{F^h_{y_2}} + \frac{F^{th}_{y_2}}{F^h_{y_1}}\Big), \tag{2.14}$$

$$\hat{\omega}_{y_1,y_2} = \omega - c_\omega \Im\Big(\frac{F_{y_1}^{\frac{dh}{dt}}}{F_{y_2}^{h}} + \frac{F_{y_2}^{\frac{dh}{dt}}}{F_{y_1}^{h}}\Big) \tag{2.15}$$

where

$$\frac{F_{y_1}^{th}}{F_{y_2}^{h}} = \frac{A_1}{A_2} e^{-i(\phi_1-\phi_2)} \frac{F_{x}^{th}}{F_{x}^{h}}, \tag{2.16}$$

$$\frac{F_{y_1}^{\frac{dh}{dt}}}{F_{y_2}^{h}} = \frac{A_1}{A_2} e^{-i(\phi_1-\phi_2)} \frac{F_{x}^{\frac{dh}{dt}}}{F_{x}^{h}}, \tag{2.17}$$

conversely for shifted $y_1(t)$ and $y_2(t)$. Consequently, the terms can be expressed as

$$\frac{F_{x_1}^{th}}{F_{x_1}^{h}} + \frac{F_{x_2}^{th}}{F_{x_1}^{h}} = \frac{A_1^2 + A_2^2}{A_1 A_2} \cos(\phi_2 - \phi_1) \frac{F_{x}^{th}}{F_{x}^{h}}. \tag{2.18}$$

$$\frac{F_{x_1}^{\frac{dh}{dt}}}{F_{x_2}^{h}} + \frac{F_{x_2}^{\frac{dh}{dt}}}{F_{x_1}^{h}} = \frac{A_1^2 + A_2^2}{A_1 A_2} \cos(\phi_2 - \phi_1) \frac{F_{x}^{\frac{dh}{dt}}}{F_{x}^{h}}. \tag{2.19}$$

The scaling factors c_t and c_ω are amplitude adjusted according to

$$c_t = c_\omega = 2\frac{A_1 A_2}{A_1^2 + A_2^2}. \tag{2.20}$$

Finally, when $\phi_1 = \phi_2$, i.e. phase synchronization, equations (2.18), (2.19), reduces to equations (2.8), (2.9), with perfect time-frequency localization to $\hat{t}_{y_1,y_2}(t,\omega) = t_0$ and $\hat{\omega}_{y_1,y_2}(t,\omega) = \omega_0$. Thus, the matched phase reassignment method is a time-frequency local measure of phase synchronization.

2.6 Rényi entropy

Measuring the entropy of a system is a way to quantify the uncertainty of that system. In the case of evaluating the synchronization between two signals, the Rényi entropy can be applied, defined as [10]

$$H_\alpha(X) = \frac{1}{1-\alpha} \log_2\Big(\int_{-\infty}^{\infty}\int_{-\infty}^{\infty} RS_x(t,\omega)dtd\omega\Big), \;\; \alpha > 2. \tag{2.21}$$

When the Rényi entropy is low, good phase synchronization has been achieved.

2.7 Finite impulse response filter

As described in the introduction to the thesis, the signals used in this project has two important properties from a signal processing perspective. The first property is that there is an envelope in the signal, corresponding to the insect's body and its flight path within the recording laser. If only this body envelope was to be analyzed no information about frequencies and phases related to the wings of the insect would be captured. The second property is that within this envelope, the contribution from

the insect's wings to the signal are captured. Higher frequencies are superimposed on the body envelope, and it is here the important information lies. This can be seen in fig. 2.3, which also was shown in the introduction:

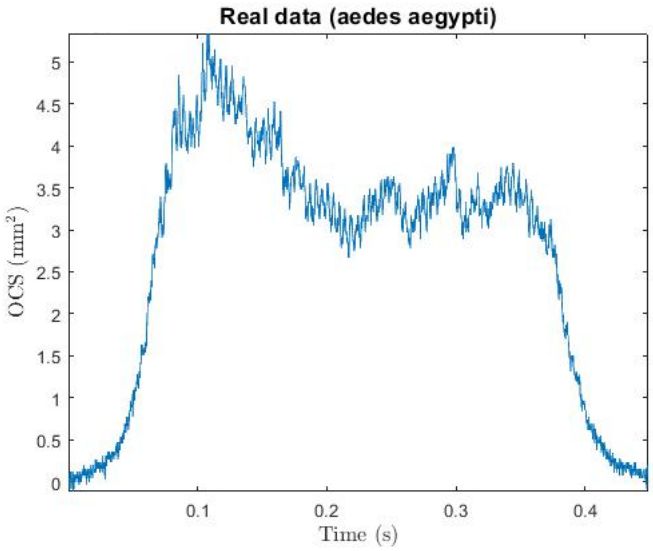

Figure 2.3: Plots of real data of yellow fever mosquito (*aedes aegypti*) with the optical cross section (OCS) measured in mm^2. Also shown in fig. 1.1.

In the image in fig. 2.3, it is clear that the signal has a general envelope, corresponding to the body part of the insect, and faster fluctuations corresponding to the wings (and noise). In order to analyze signals like this with the methods mentioned above, the body part of the signal will be filtered out. The frequencies of the body envelope are, in relation to the wings, low and applying a low-pass filter is therefore well suited for the task of filtering out the body.

A digital low-pass Finite Impulse Response (FIR) filter will be designed in order to capture the body part characteristics of the signal, and then removed from the signal by subtracting this part. The process will be as follows:

1. `Design an N-order digital FIR filter for the body part of the signal.`
2. `Filter out this part from the signal, thus creating a "body-part only" signal.`
3. `Subtract this body-part signal from the original signal, removing the body envelope.`

2.8 Gaussian envelope

After filtering out the body part of the signal, the remaining signal is what is relevant for this thesis. It contains the information about frequencies and phases. In order to apply the algorithm described above, the signal has to have a shape that is well replicated by the matched phase reassignment algorithm. One way to shape this

data is to multiply a segment of the signal with window $w(n)$ with a characteristic look. For example, a Gaussian window can be used, creating a Gaussian envelope. This does not change the overall behavior of the signal since the frequencies and the phases are captured within this envelope. As described in the theory section, the matched phase reassignment is suitable for transient signals. It is known that the matched phase reassignment works especially well with a Gaussian envelope [5], which also is a simple envelope to implement.

The Gaussian window is defined as [11]

$$w(t) = \exp\Big(-\frac{1}{2}\Big(\frac{t - t_1/2}{\alpha}\Big)^2\Big), \tag{2.22}$$

where t_1 represents the length of the signal. The parameter α is proportional to the width of the window, where a larger α yields a longer signal. Different values of α will be investigated. It has the well known bell-shaped curve seen in fig. 2.4:

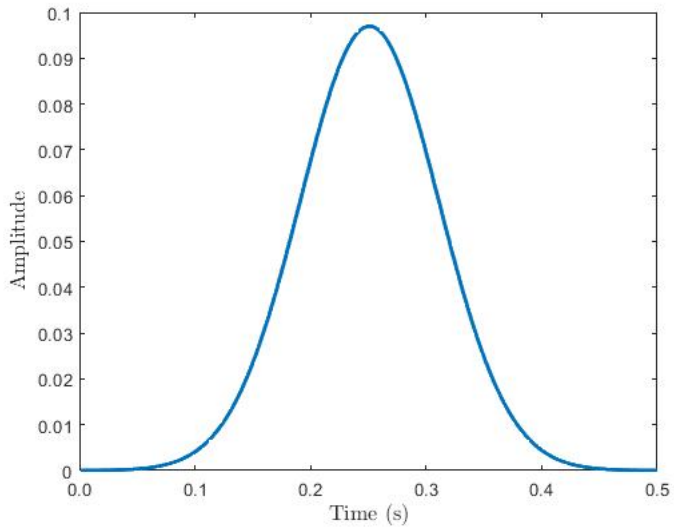

Figure 2.4: Gaussian window

2.9 Wavelets and denoising

It is known that the matched phase reassignment is sensitive to noise [12]. A natural way to improve the results is thus to try to denoise the data. The scope of denoising in this thesis is to implement a method that hopefully improves the phase estimations. The method of denoising has been chosen to be denoising with wavelets. A wavelet is a type of basis function for the wavelet transformation. The energy of the wavelet is concentrated in time which enables better representation of transient, non-stationary signals [13], thus making it well suited for this thesis. Wavelets enable the signal to be split into different levels of resolution, varying from large scale ("approximation") to small scale ("detail") level.

2.9.1 Wavelets

The Wavelet Transform
The process of working with wavelets is very similar to when working with the Fourier transform. Just as with the Fourier transform, a signal is transformed from the real domain to the corresponding target domain, in this case using the wavelet transform. Within the wavelet domain, the signal properties are altered to suit a specific purpose, after which it is then transformed back to the original real domain using the inverse wavelet transform.

A family of wavelets $\psi_{s,\tau}(t)$ is defined by scaling and translating the mother wavelet $\psi(t)$ with the continuous-valued parameters $s > 0$ and τ,

$$\psi_{s,\tau}(t) = \frac{1}{\sqrt{s}}\psi\Big(\frac{t-\tau}{s}\Big). \tag{2.23}$$

The continuous wavelet transform (CWT) $w(s,\tau)$ of a continuous-time signal $x(t)$ is defined as,

$$w(s,\tau) = \int_{-\infty}^{\infty} x(t)\frac{1}{\sqrt{s}}\psi\Big(\frac{t-\tau}{s}\Big). \tag{2.24}$$

This is the correlation between $x(t)$ and a scaled and translated version of $\psi(t)$.

The function $x(t)$ can be reconstructed using the inverse wavelet transform,

$$x(t) = \frac{1}{C_\psi}\int_{-\infty}^{\infty}\int_{0}^{\infty} w(s,\tau)\frac{1}{\sqrt{s}}\psi\Big(\frac{t-\tau}{s}\Big)\frac{d\tau ds}{s^2}, \tag{2.25}$$

where

$$C_\psi = \int_0^\infty \frac{|\Psi(\Omega)|^2}{|\Omega|}d\Omega < \infty, \tag{2.26}$$

and $\Psi(\Omega)$ denotes the Fourier transform of $\psi(t)$.

Multiresolution Signal Analysis
As explained in the introduction to wavelets, a signal can be viewed as a sum of smoother parts and more detailed parts. In this thesis, the smoother part corresponds to the insect's body and the more detailed part corresponds to the wings and noise.

At scale j, the approximation of a signal is denoted as $x_j(t)$. At scale $j+1$, the approximation is defined as $x_{j+1}(t) = x_j(t) + y_j(t)$, where $y_j(t)$ represents the details at scale j.

By adding more detail to $x_j(t)$, as the resolution approaches infinity, a signal is obtained which involves a smooth part and the detailed part,

$$x(t) = x_j(t) + \sum_{l=j}^{\infty} y_l(t). \tag{2.27}$$

2.9.2 Denoising using wavelets

As previously mentioned, the coefficients relating to noise are often observed in the finer scales of the signal. Denoising is thus an operation where the detail coefficients are altered in order to produce a smoother signal, hopefully obtaining noise reduction without corrupting the signal. The procedure can be summarized in three steps,

```
1. Calculate the discrete wavelet transform of the noisy signal.
2. Modify certain coefficients, fitting the task at hand.
3. Reconstruct the signal with the modified coefficients.
```

For denoising, thresholding can be used to modify coefficients below a certain threshold. After the modification of the coefficients, the signal is inversely transformed back and hopefully a denoised signal is obtained.

The wavelet transform vector $\mathbf{w_N}$ is introduced,

$$\begin{aligned}\mathbf{w_N} =&[w_1\ w_2\ \dots\ w_N]^T = \\ &[c_0(0)\ d_0(0)\ d_1(0)\ d_2(0)\ \dots\ d_{(log_2N-1)}(log_2N)]^T,\end{aligned} \tag{2.28}$$

The finer details are at the end of the vector $\mathbf{w_N}$, and thus a threshold can be introduced to modify these detail coefficients.

Hard thresholding
In this thesis, denoising by hard thresholding will be used, defined by

$$\breve{w}_i = \begin{cases} w_i, & |w_i| \geq \eta_T, \\ 0, & |w_i| < \eta_T, \end{cases} \tag{2.29}$$

where η_T is a threshold.

The threshold η_T will be chosen as a fixed constant.

In order for the denoising technique to work well, the length of the signal needs to be a multiple of 2, i.e. 2^j, $j = 1, 2, 3, ...$ This is due to the strong dyadic nature of the algorithm and the consequence is that for the signals that requires denoising, the length of the signal needs to be shortened to fulfill this requirement on length.

Chapter 3

Data Simulation

3.1 Simulating the insect

The goal of the thesis is to apply the algorithm on real data. Before that can be done the model needs to be assessed which will be done on simulated data made in Matlab. The procedure of simulating the insect will be done in two steps. The first step is to produce the actual signal which has both the body part of the signal and its wings. Then, the body will be filtered out in order to obtain just the wing-part of the signal.

Real data has the general look seen in fig. 3.1:

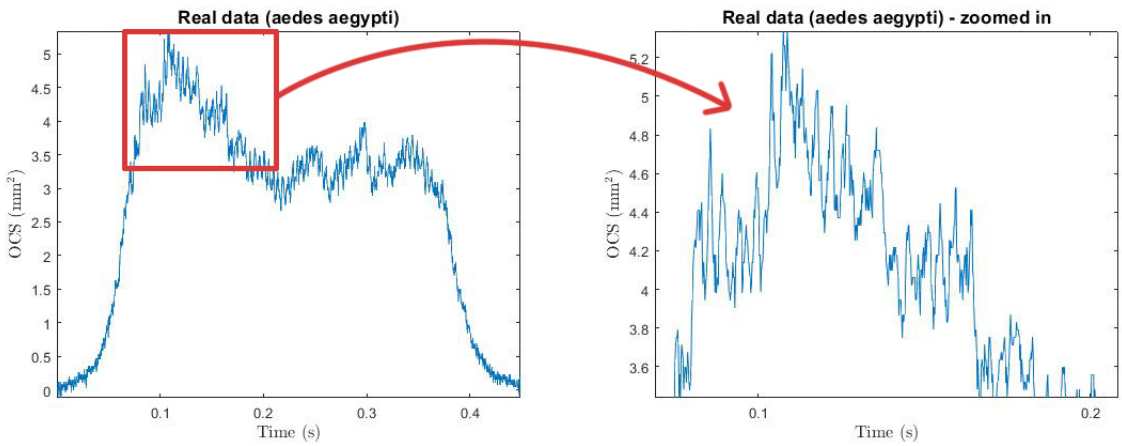

Figure 3.1: Plots of real data of yellow fever mosquito (*aedes aegypti*), red part zoomed in for clarity and to show the part of the signal that arises from the wings more clearly. Note that the body envelope isn't constant but varies with the flight path.

As can be seen in the left of fig. 3.1, the signal is composed of an envelope representing the body of the insect, and detailed variations, as zoomed in on the right figure, representing the wing part of the signal.

The body part of the signal will be simulated as

$$y_{body}(t) = \sum_{b=0}^{\#\text{components}} A_b \cos\left(2\pi(f_b \cdot t + \phi_b)\right), \tag{3.1}$$

where A_b represents the amplitude of the signal, f_b its frequency and $\phi_b \in [0, 1]$ the corresponding phase. The number of overtones can be changed to create a suitable signal, and for this thesis five overtones has been used. The main amplitude has been set to 50, and the lowest frequency has been set to 20 Hz. The phases are randomized. The most important part of the simulation of the body is to not use too high frequencies, since this might become close to the fundamental wing beat frequency.

Furthermore, the wing part of the insect is created in the same manner,

$$y_{wings}(t) = \sum_{n=0}^{\#\text{overtones}} A_n \cos\left(2\pi(f_n \cdot t + \phi_n)\right). \tag{3.2}$$

Here, the amplitude corresponding to the fundamental frequency is set to 10, which means it is $\frac{1}{5}$ the size of the body. The amplitudes of the overtones will be divided with its number, i.e. $A_n = \frac{10}{n}$. The fundamental wing beat frequency f_1 will have a value corresponding to real species fundamental wing beat frequency, e.g. yellow fever mosquito has a fundamental wing beat frequency around 200 Hz. The phases are randomized, but now stored in a vector in order to be able to assess the results produced by the algorithms. The same goes for the frequencies, which are also stored enabling evaluation of results.

At this point, a clean signal representing a flying insect has been created. In order to represent real data, noise is an important factor and that is quantified using signal-to-noise ratio (SNR),

$$\text{SNR} = 10\log_{10}\left(\frac{\int_{t_0}^{t_1} y^2(t)dt \cdot \frac{1}{t_1 - t_0}}{\sigma^2}\right) \iff \sigma = \sqrt{\frac{\int_{t_0}^{t_1} y^2(t)dt \cdot \frac{1}{t_1 - t_0}}{10^{\text{SNR}/10}}} \tag{3.3}$$

In order to evaluate how well the algorithms work on different noise levels, different levels of SNR will be used.

The final simulated data signal can thus be written as

$$y(t) = y_{body}(t) + y_{wings}(t) + \sigma e(t), \tag{3.4}$$

where $e(t) \sim \mathcal{N}(0, 1)$ represents white Gaussian noise.

A simulated signal can be seen in fig. 3.2:

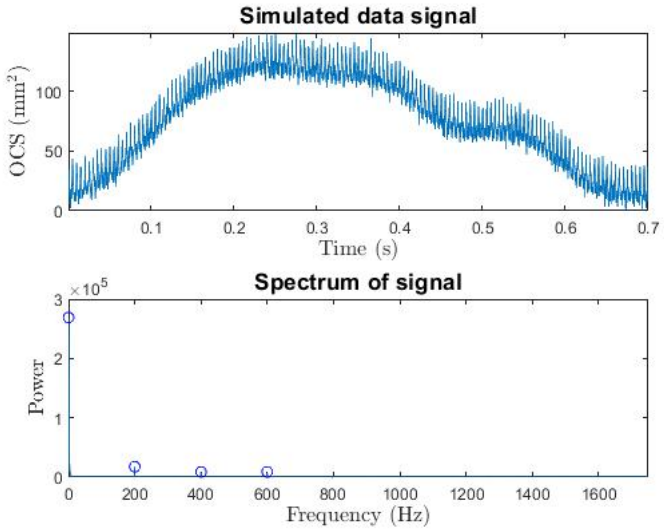

Figure 3.2: An example of a simulated data signal with its corresponding frequency component spectrum.

The simulated signal in fig. 3.2 has a length of 0.7 seconds. For real data, this time varies but 0.7 seconds corresponds well to how long the insect stays within the laser. Furthermore, the simulated signal has a fundamental wing beat frequency of 200 Hz, with a sampling frequency of 5000 Hz, an SNR level of 20 and the wing-part has two overtones.

It is clear, both from the image of the signal and its spectrum, that there is a part clearly defined for the body part of the insect, and a wing part.

3.2 Filtering

The first step of manipulating the data is to filter out the body part of the signal. A low-pass filter will be used to separate the body from the rest of the signal. This will then be subtracted from the signal in order to obtain the wing part of the body, as explained in the theory section. Using the same simulation settings as above, the filtered signal can be seen in fig. 3.3.

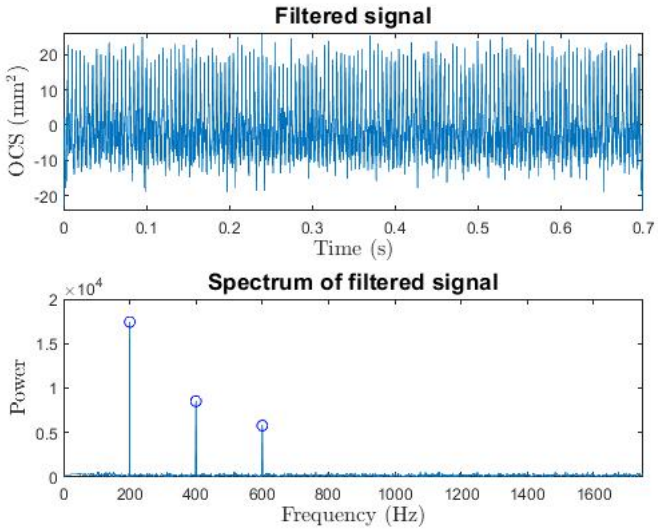

Figure 3.3: Filtered simulated signal with its corresponding frequency component spectrum.

Here, a low-pass filter with cutoff frequency at 100 Hz was applied. As can be seen in fig. 3.3, the body part of the signal has clearly been removed. The spectrum also shows clear peaks for the fundamental wing beat frequency and its two overtones, with the body part removed.

3.3 Denoising

As also can be observed in fig. 3.3, the signal is still quite noisy. Therefore a noise reduction technique is applied, in this case wavelet denoising via hard thresholding. An example of obtained denoising can be seen in fig. 3.4,

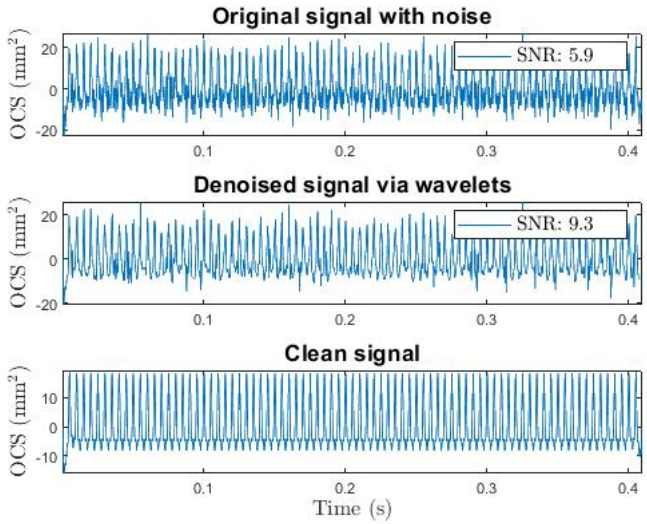

Figure 3.4: A filtered simulated signal with noise together with the denoised signal and the clean signal.

The SNR has increased from 5.9 to 9.3, in this example.

The SNR is harder to calculate for real data, since SNR is the ratio between the power of the clean signal, and the power of the noise,

$$\text{SNR} = \frac{P_{signal}}{P_{noise}}, \tag{3.5}$$

where P_{signal} is the clean signal, without any noise, and P_{noise} is the noise. Both of these need to be measured at the same, or an equivalent, time which is hard to do for the real data. Therefore, an empirical constant will be used for the denoising of real data if the denoising is deemed successful on simulated data. An example of this can be seen in fig. 3.5

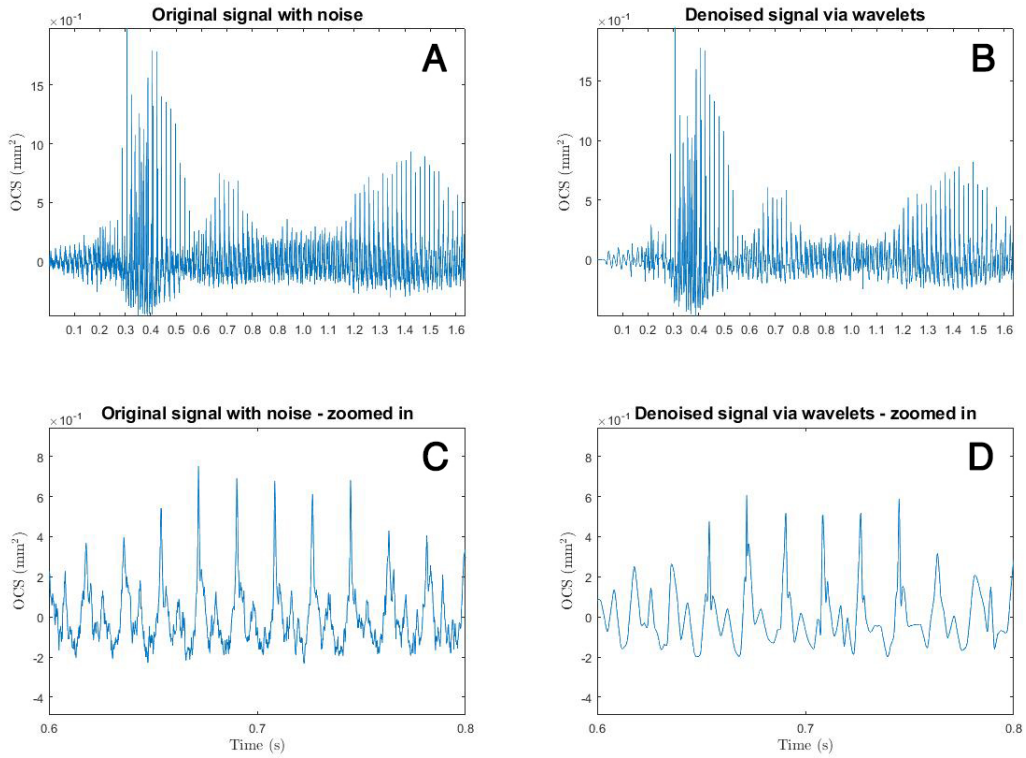

Figure 3.5: Denoised filtered real signal. (A): Original signal with noise. (B): Denoised signal via wavelets. (C): Original signal with noise - zoomed in. (D): Denoised signal via wavelets - zoomed in.

3.4 Using windows

After filtering and denoising, the Gaussian window is applied to the signal. It is important to capture enough information in order for the algorithms to work properly, meaning that the width of the window needs to be determined. Furthermore, the simulated signal is relatively long compared to what the signal will be after applying a window. Therefore, a lot of information could go lost. To prevent this, the signal will be multiplied with the same window in evenly distributed positions throughout the signal. This allows for capturing of more information than just taking out one segment of the signal. These segments will individually be evaluated, producing frequencies and phases. The median of the results will then be taken as the end result. The algorithm for applying the window is as follows.

```
1: Decide how many segments of the signal to be used, N segments.
2: Create the window.
3: Multiply the signal with evenly distributed windows, creating
   N segments of the signal.
```

This is illustrated in the fig. 3.6:

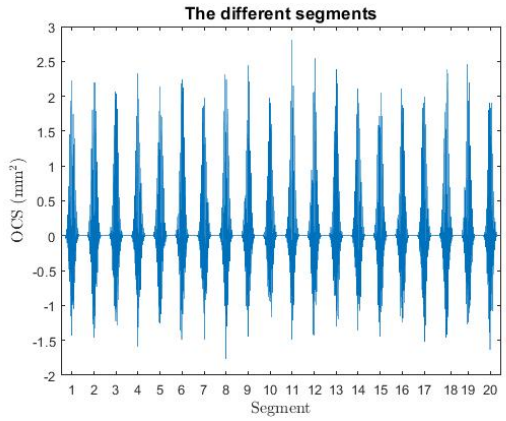

(a) 20 different segments of the signal.

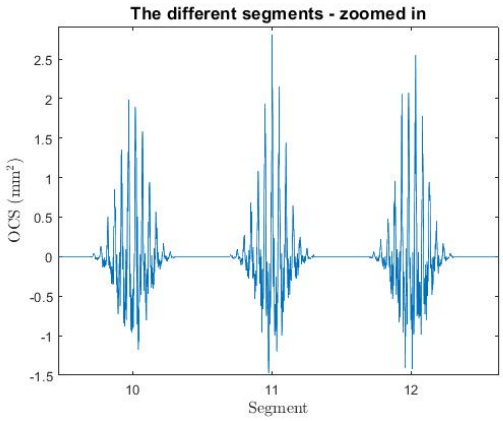

(b) Three of the 20 segments - zoomed in for visuality.

Figure 3.6: A filtered and denoised signal multiplied with a Gaussian window at 20 different locations, producing 20 different segments of the signal.

The segments in the above figure has an interval length of 60 ms. This interval length is not definitive and can be changed in order to possibly produce better end results.

Multiplying the signal with a Gaussian window does not change the signal's fundamental properties. The frequency components and the relative phases will be captured within the window and the properties will not change. The initial phase might be altered due to removal of information in the process of multiplying with the window, but the relative phases remains the same.

3.5 Downsampling

The real data is recorded with a frequency of 20 kHz. In order to get the frequency down to a level that the matched reassignment method works better on, downsampling will be done. In order to avoid aliasing when downsampling, Matlab's function 'decimate' will be used. This function applies a low-pass Chebyshev Type 1 infinite impulse response filter of order 8 to prevent aliasing from occurring [14].

3.6 Running the algorithm

At this point, the signal has been manipulated enough so that it can be evaluated by the algorithms. The insect has been simulated, the body filtered out, denoising was applied and segments were taken out with Gaussian windows. These segments will now be evaluated and the matched reassignment and matched phase reassignment methods will be applied to these segments. As previously stated, the end result is the median of the relative phases of each segment.

3.7 Identifying fundamental frequency and harmonics

The matched reassignment method will be applied to the different segments of the signal. This will produce a number of different frequencies, each corresponding to a peak in the spectrum. An example of this can be seen in fig. 3.7:

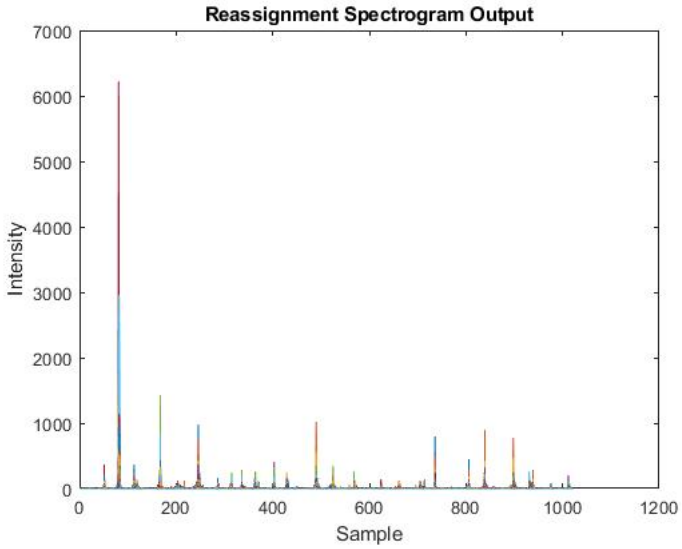

Figure 3.7: Reassigned spectrogram output.

By sorting these frequencies based on intensity, the fundamental frequency and its overtones are identified. The process is as follows:

1. Decide how many frequencies to estimate, K frequencies.
2. Estimate the frequency distribution using matched reassignment.
3. Sort the frequencies based on intensity.
4. Use the top K frequencies as input for the matched phase reassignment.

3.8 Estimating the relative phases

Once the frequencies have been estimated by the matched reassignment, they are used in order to create surrogate data,

$$g(t) = \cos(2\pi(\hat{f}_k t + \phi_i)). \tag{3.6}$$

Here, $\hat{f}_k$ corresponds to the frequencies that the matched reassignment estimated. ϕ_i corresponds to a "test phase". This means that the more surrogate data that is generated, more precise estimation of the phases will be obtained.

This surrogate data is then multiplied by the same Gaussian window as the original signal was, and then compared with the original signal using the matched phase reassignment method. For each surrogate data, the Rényi entropy is calculated and

the test phase that produces the lowest entropy is deemed to be the correct phase. An example of how the Rényi entropy could look is presented in fig. 3.8:

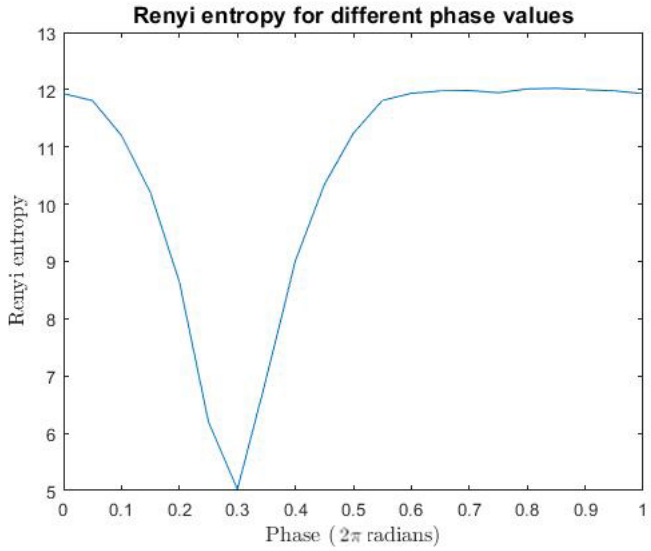

Figure 3.8: Example of how the Rényi entropy varies for different phases.

In in fig. 3.8, 0.3 would have been deemed to be the true phase.

The process of estimating the phases is as follows:

1. Based on the top K frequencies estimated by the matched reassignment, create surrogate data with the same frequencies.
   Let the surrogate data be initiated with a test phase of 0, and then incrementally increase the phase, with a pre-defined step size.
2. Multiply the surrogate data with the Gaussian window, replicating the look of the original data.
3. Calculate the matched phase reassignment, based on the original signal and surrogate data as input.
4. Calculate the Rényi entropy.
5. Choose the test phase that produced the lowest Rényi entropy as the true phase.

3.9 Sorting the data

A problem that can arise throughout this process is that the fundamental frequency of the signal is not the one that has the highest intensity. This means that the fundamental frequency will be estimated wrongly, since the matched reassignment will estimate the fundamental frequency to be the frequency with the highest intensity. This problem is solved by sorting the results based on the lowest frequency, instead of highest intensity. Sorting in an ascending order, and doing the same for the phases, will correct this issue and produce results that are in line with requirement that the overtones are by definition higher than the fundamental frequency.

The process is as follows:

1. Go through frequencies list, for each frequency check if it is
   in correct place.
   Otherwise adjust accordingly.
2. For each adjusted frequency, also adjust the corresponding phase.

When the sorting of the data is complete, the complete process from simulating data to getting estimations of frequencies and phases is complete.

Chapter 4

Results from simulated data

4.1 An initial assessment of the algorithm

To get an estimation for what the algorithm can handle in terms of number of overtones, noise, sampling frequency and so on, initial tests were done to see where it performs the best. This will provide an area of settings where the method works well and will thus be a focus area on how well the algorithm actually performs, with more statistical robustness.

4.1.1 Restrictions in simulations

The variable parameters when simulating the data include the fundamental wing beat frequency of the insect, number of overtones, noise, sampling frequency, envelope settings, number of segments, phase step and so on. The most significant parameters to look at are the FWBF, number of overtones, noise and the sampling frequency. The other settings are also important. However, due to the high time consumption of running a simulation, these were set as fixed values based on empirical data that continuously during the thesis work has proven to work well.

For the simulation of data, it is assumed that the insect stays within the physical recording laser for approximately 0.7 seconds. This has been discussed previously, and this number stems from real data and the consequence of having a fixed time is that a lower sampling frequency will provide a lower resolution of the signal, and vice versa. It is worth reminding the reader that these 0.7 seconds will be shortened to produce a length of the signal corresponding to 2^j, $j = 1, 2, 3, ...$, if denoising is applied.

It is important to have a varying sampling frequency since this has an impact of how well the different frequencies can be estimated. A higher sampling frequency might provide better results for the higher overtones, but the details of the lower frequencies can be lost. The same way for lower sampling frequencies providing good estimations for low frequencies but for the higher overtones the details might get lost due to the low sampling frequency.

As previously mentioned in the report, the phases are periodic. This means that,

$$\cos\left(2\pi(f+\phi)\right) = \cos\left(2\pi(f+2\phi)\right), \tag{4.1}$$

where ϕ is a phase between 0 and 1. Since 2π is factored out, the estimated $\hat{\phi}$ corresponds to unit 2π radians. When estimating these phases, the consequence is that 0 and 1 are both correct results. In order to illustrate this problem, the two images in fig. 4.1 represents phases on the unit circle. The red line moves along the unit circle's edge, starting with an angle of 0 radians (i.e., lying on the positive real axis). When the red line has moved along the whole circle, thus completing a full "lap" on the circle, the phase is 2π. Since it moved a full lap, however, the phase is also 0, which is where the periodicity lies. This is illustrated in fig. 4.1:

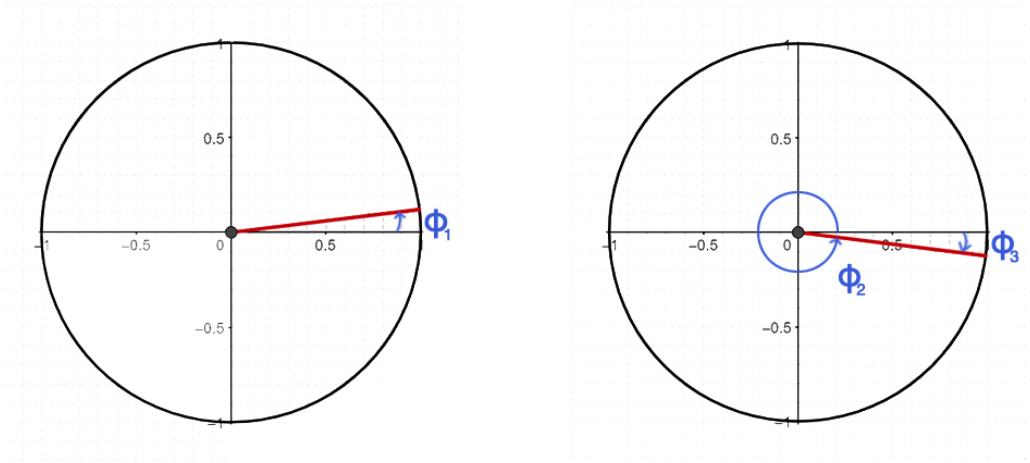

(a) Phase, ϕ_1 is close to 0. (b) Phase, ϕ_2 is close to 2π, ϕ_3 is close to 0.

Figure 4.1: Illustration of the phase problem.

In fig. 4.1a, it is clear that ϕ_1 is a phase that takes a small value, and is close to 0. If letting ϕ_1 grow larger, the red line will move along the unit circle and eventually end up as in fig. 4.1b, where ϕ_2 now represents a larger phase that is close to 2π. The problem is that if a phase approximation method estimates ϕ_2, when it should estimate ϕ_1, the error will be deemed to be very large (almost 2π error, the maximum value it can take). However, ϕ_3, represented in fig. 4.1b, is much closer to ϕ_1 than ϕ_2 while they are both representing the same phase. The fundamental issue lies in how to evaluate a phase estimation. As an example, let a signal have one overtone, i.e. the fundamental frequency and one overtone and assign them some appropriate numbers,

$$\begin{aligned} \phi_1 &= 0.05 \\ \phi_2 &= 0.3. \end{aligned} \tag{4.2}$$

Looking at the phases above, ϕ_1 is intentionally assigned a number close to zero. The absolute value of the phase difference between ϕ_1 and ϕ_2 is $|\phi_1 - \phi_2| = 0.25$. If the algorithm instead estimates $\hat{\phi}_1 = 0.95$, which in the perspective of phases is very close, with a distance of 0.1 to the actual value (and not 0.9), then the evaluation

will point towards quite a bad model that does not work well. In reality, it has estimated the phase much closer than what the actual distance will say. This is a tough problem to solve, especially when analyzing real data where no prior information about the phases exists. For the sake of simplicity and avoiding this problem, the phases in simulation will be restricted to the interval $[0, 0.5]$. Since the phases now lie far away from this border case, there is no risk of the results getting affected and confused around 0. This restricts the model, but for evaluation purposes this is motivated by actually wanting to get a non-biased result on how well the phase estimation works.

Lastly, the phase step will be set to 0.1. This means that the phases to be tried will be six phases between 0 and 0.5. The simulated signals will have its phases in that same interval, as well, so that it is possible to estimate the exact phase with a step size of 0.1. This is a large step, but sufficient for an initial assessment. This reduces the run times drastically and will still provide a rough estimation of how the algorithm behaves in response to the different settings.

4.1.2 Initial results of the simulations

The first initial simulations were done to get an approximate image of what the algorithm can handle. The evaluation look at the median of the results, with five runs per setting. This means that if number of overtones is to be changed, five runs on each change will be made.

The process of evaluating the performance on different parameters is as follows:

1. Initiate variables.
2. Choose one of the variable parameters and let it vary, setting the others as fixed. Evaluate.
3. Let next parameter vary, with rest fixed. Evaluate.
4. Repeat step 3 until all parameters have been evaluated.

This will be done by iteration in order to get a good initial assessment in which areas the algorithm performs well.

The first initial runs were with a fundamental wing beat frequency of 200 Hz, sampling frequency F_s of 1000 Hz, no noise and a varying number of overtones, K. The results can be seen in the fig. 4.2:

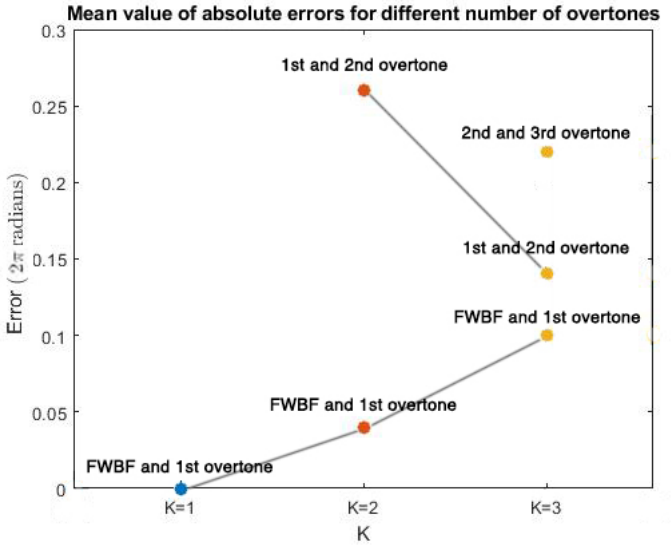

Figure 4.2: Mean value of absolute errors in phase estimation for different number of overtones.

In fig. 4.2, the blue dot corresponds to the signal with one overtone, i.e. the fundamental frequency and one overtone. It represents the error of the phase difference between the fundamental frequency and the overtone. In the same way, the red dots correspond to the signal with two overtones, and the yellow with three overtones. As can be seen, the accuracy of the approximation of the first phase difference, i.e. between fundamental frequency and its first overtone, seems to be decreasing for increasing values of K. This is probably due to a low sampling frequency F_s which corrupts the finer details of the signal thus suppressing the resolution of higher overtones. The actual values can be found in the appendices.

The next step is raising the sampling frequency, with four tones (fundamental frequency and three overtones) and rest of the parameters stay the same as in previous test. The results can be found in fig. 4.3:

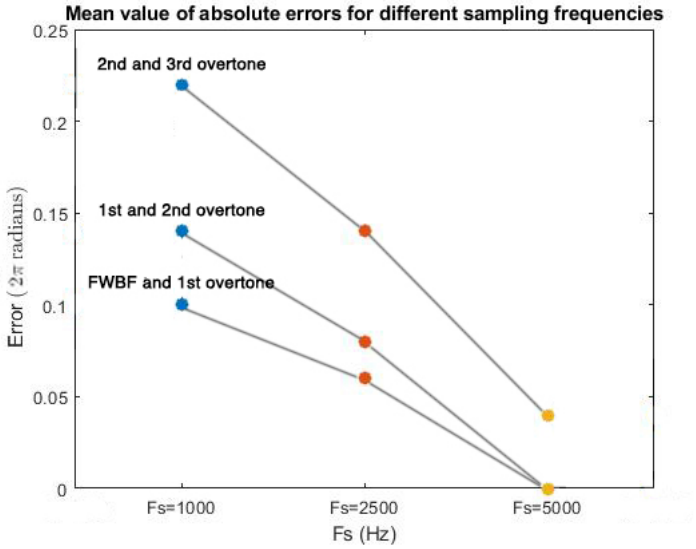

Figure 4.3: Mean value of absolute errors in phase estimation for different sampling frequencies but the same FWBF.

Note: There are two yellow dots corresponding to an error of 0.

In the fig. 4.3, the same color-coding applies as in the previous figure. For the yellow dots, the phase difference between fundamental frequency and its overtone, and the phase difference between overtone 1 and 2 both have zero error. The actual values can be found in the appendices.

The next step is to raise the fundamental wing beat frequency. The results can be seen in the fig. 4.4:

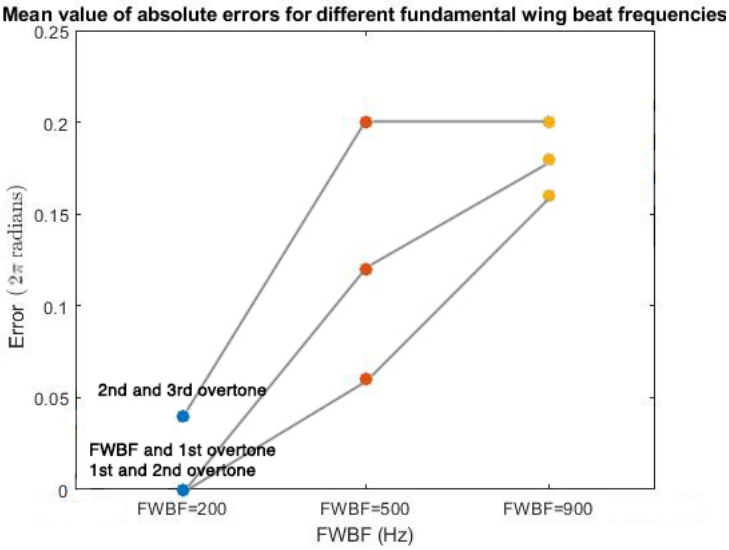

Figure 4.4: Mean value of absolute errors in phase estimation for different FWBF.

Note: There are two blue dots corresponding to an error of 0.

As can be seen in fig. 4.4, the errors is the lowest for a fundamental wing beat frequency of 200 Hz. The phase difference between the fundamental frequency and its overtone, and the first overtone and the second both have zero error. The values can be found in the appendices.

Lastly, different noise levels will also be tried. For each of the different SNR levels, $K = 3$ will be tried, i.e. the fundamental frequency and two overtones. The sampling frequency will be 5000 Hz and the fundamental wing beat frequency will be 200 Hz. The algorithm is known to be quite sensitive to noise, so the SNR levels of $40, 30, 20$ and 10 will be tried. The results can be seen in fig. 4.5:

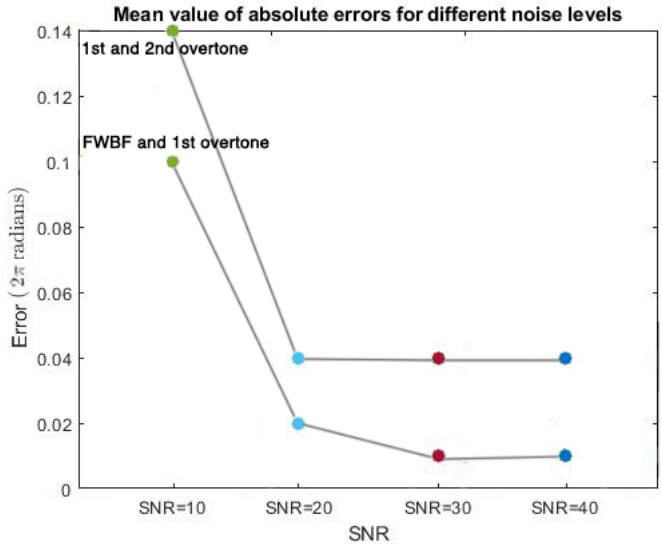

Figure 4.5: Mean value of absolute errors in phase estimation for SNR FWBF.

As can be seen in fig. 4.5, the algorithm performs quite well for SNR levels down to 20, but lower than that it seems to perform worse. It can also be observed that the estimation of the first phase difference, i.e. between fundamental frequency and its first overtone seems to be best for SNR levels of around 30 to 40.

4.2 Final evaluation of the algorithm

After this initial assessment of how the algorithm works with different sampling frequencies, noise levels, number of overtones and fundamental wing beat frequencies, an area of focus was determined. From the values above, it was decided to evaluate the settings of $F_s = 5000$ Hz, with a noise level of SNR $= 15 - 20$, a fundamental wing beat frequency of FWBF $= 200$ Hz and two overtones (the fundamental frequency and two overtones), in more detail.

Doing 100 simulations on each parameter, the results can be seen in fig. 4.6:

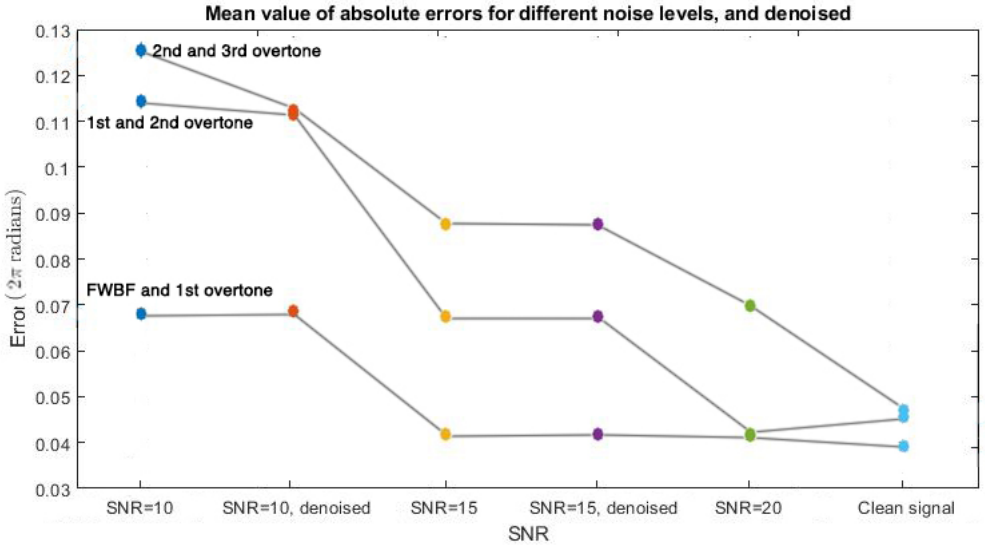

Figure 4.6: Mean value of absolute errors in phase estimation for different SNR with both denoised and undenoised signals.

Note:
There are two orange dots corresponding to an error of around 0.11.
There are two green dots corresponding to an error of around 0.04.
There are two blue dots corresponding to an error of around 0.05.

As can be seen from fig. 4.6, the algorithm performs the best for a clean signal, and it can estimate the phase differences quite well up to three phase differences.

The algorithm was also tested for 100 simulations on a signal with FWBF of 900 Hz and a noise level of SNR 20. The plot in fig. 4.7 shows the same simulations for a signal with FWBF of 200 Hz, for comparison:

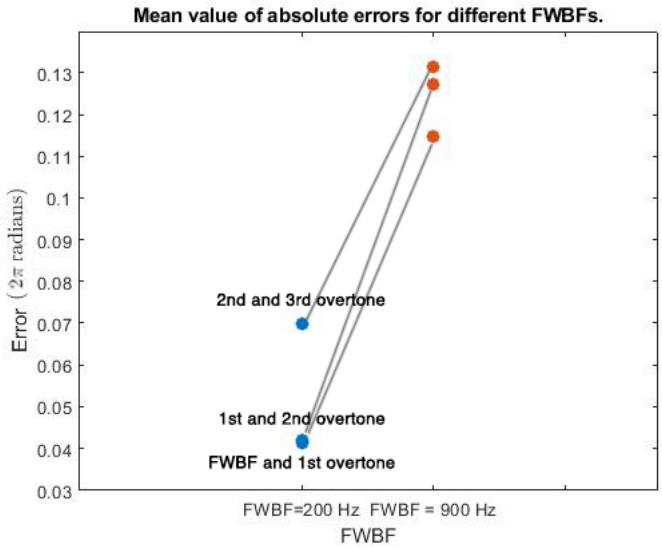

Figure 4.7: Mean value of absolute errors in phase estimation for different FWBF.

Note:
There are two blue dots corresponding to an error of about 0.04.

As can be seen in fig. 4.7, there is a big difference in how the algorithm works for FWBF 200 Hz and FWBF 900 Hz. This was also the suspicion from the initial test runs in the previous subsection of the report.

Chapter 5

Obtaining Lab Data

5.1 Theory

5.1.1 Laser-insect interaction

In order to study insects in vivo, that is to say to study living insects, with a high temporal and spatial resolution traditional methods such as traps cannot be used since they cannot give any feedback until they are emptied. Apart from being quite labour intensive they are also very intrusive to the insects. In order to reduce both the labour intensiveness and the intrusiveness to the insect measurements lidar can be used. To this end laser in the infrared spectrum can be used since many insects cannot see electromagnetic radiation in that part of the spectrum[15]. Here continuous-wave (CW) lasers with wavelengths in the near infrared (NIR) and in the short-wave infrared (SWIR) were chosen. For the NIR the wavelength 808 nm was picked which can be measured with low cost Si-CMOS, something that also is useful for recording with cameras and for the SWIR 1320 nm was chosen. Another trait of 808 nm is that it can be absorbed by melanin in the insect which is something that reduces the amount of backscattered light from the insect. The melanin in insects occurs in the cuticle and in general the highest degree of melanization occurs around the head. The melanization in the body may vary between different insects which in theory allows for distinction between species. There is however also melanin in the veins on the wings on insects as well. In contrast 1320 nm light is unaffected by melanin.

The degree polarized light becomes depolarized largely depends on how many times the light bounces in the insect which in turn depends on how thick the part the light hits is. As a result the wings, which are rather thin, tend to reflect much more linearly polarized light than the much thicker body. To the degree that depolarized light is backscattered it arises mostly from the veins in the wings which tend to be thicker. The thickness of the wings will also determine which wavelength will have constructive interference which will result in stronger backscattered signals for the wavelengths. For wing thickness of 395 and 659 nm the 808 nm laser will interfere constructively [4]. Due to the small size of the insects they will be flooded with photons and a significant amount of light will be forward scattered.

5.1.2 Modulation

When a flying insect is crossing a laser beam backscattered light will arise from both the body and the wings, which can be recorded by a photodiode. The amount of backscattered light from the body will be largely dependent on the heading of the insect and the generated signal will tend vary slowly as the insect flies through the beam. In contrast the recorded signal arising from the wings will have an oscillatory appearance due to the oscillatory nature of the wing beat frequency. Even the wing signal will however be dependent on the heading of the insect as it will determine how much light is backscattered [4].

5.1.3 3D reconstruction

By using a camera and a mirror a 3D space can be reconstructed by comparing the location in of an object in direct vision and the reflected image. This is done by first creating a coordinate system where objects are placed and measuring their position, thereafter the indices of pixels in the camera is written down. After that a multivariate regression is done on the pixel indices.

5.2 Test chamber setup

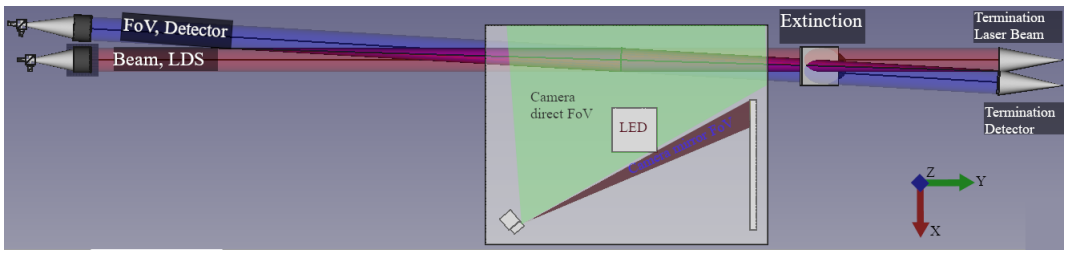

Figure 5.1: The setup seen from above. Note the coordinate system in the bottom right corner.

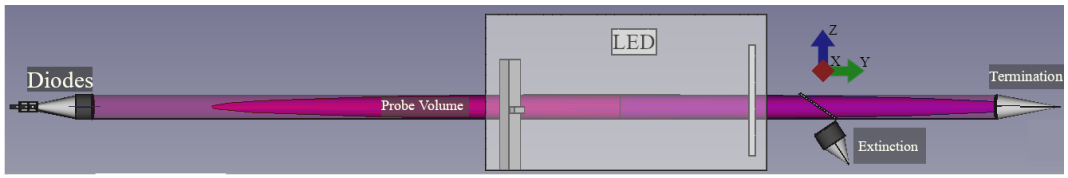

Figure 5.2: The setup seen from the side. Note the coordinate system.

In order to record specific insects in a controlled environment a setup was built, see fig. 5.1 and fig. 5.2 for a sketch. The (CW) laser diodes produced linearly polarized light and used a dichroic beam splitter in order to overlap the two laser beams. The laser diode producing 808 nm (CNI, MDL-H-808) was operated at 5 watt and the laser diode producing 1320 nm (Seminex, 4PN-116) was operated at 4 watt. The beams were collimated to a beam of about 7.6 cm in diameter using a plane

List of parts in the test chamber setup	
1	Laser diodes
2	Photodiodes
3	Probe volume
4	Camera and camera pillar
5	LED
6	Mirror
7	Extinction optics
8	Temination

Table 5.1: A table of a few parts the setup shown in fig. 5.1 and fig. 5.2 consists of.

concave lens. Two sandwiched photodiodes (Hamamatsu, K1713-09) of silicon (Si) and indium gallium arsenide (InGaAs) were placed next to the laser diodes close to parallel in order to record backscattered light and used a plane concave lens with the same diameter to focus the light on the diodes. They also used a polarization beam splitter in order to allow one of the sandwiched Si/InGaAs to record the co-polarized light and the other to record the de-polarized light. The probe volume is the result of the overlap between the laser beam and the photodiodes field of view which means that any recorded signal from the photodiode will come from the probe volume. The centre of the probe volume, and it's greatest radius, is in the middle of the test chamber. In order to reduce background noise a longpass filter with the cut-off wavelength 780 nm (Edmund Optics, RG780) was also placed in front of them. The LED light was used in order to fool the insects to think there was sun light which was supposed to increase the amount of flying. The camera was set up in the corner of the box in order to see both the scattered light directly as well as the scattered light reflected in the mirror. The camera (Basler, acA1920-155um) was run at 156 frames per second and was covered with a longpass filter (Edmund Optics, RG780) to get rid of the light from the LED. The mirror was placed as close to vertically as possible. A fraction of the light that exited the box was reflected by a glass pane placed at Brewster's angle. This light was in turn focused onto a photodiode (Thorlabs, DET10A/M) covered with a longpass (Edmund Optics, RG780) and optical density filter (Edmund Optics, OD 1.0) allowing the recording of the extinction. The termination or beam dumps were used to minimize the background noise and were constructed using neoprene. There was separate beam dumps for the laser beam and the detector in order to further reduce the amount of background noise in the signal.

5.3 Software

To record the signals from the photodiode and the images from the camera the software labVIEW was used. The software needed a way to correlate the images taken with the data acquired so timestamping the data files generated by the camera as well as the photodiodes was based on the computers internal clock which had a precision of one millisecond. In order to reduce the data stored by the program the

images had to reduced to a smaller size. To that end the camera images were divided in to two parts, one that recorded the beam and the other the mirror, which were then searched for the highest pixel value. If the highest pixel value in the image from the mirror was above the threshold an area around the pixel would be stored from both the mirror and the direct image as well as the indices for the highest pixels. The centre of mass of the matrix was calculated which together the indices of the pixels with the highest value was used to calculate the 3D coordinates. The coordinate system was defined as in fig. 5.1 and fig. 5.2.

The data from the photodiodes was recorded at 20 kHz and saved the recording as a new file every 10 seconds. To reduce the amount of space required to store the data files they were filtered after the measurement had been completed. The filter used a threshold based on the mean of the signal from the coherent Si photodiode plus 0.1. The reason for basing the filter on the coherent Si signal was due to the fact that the camera could see 808 nm light whereas 1320 nm light would be invisible. The choice to base the filter on the mean of the signal plus 0.1 was arbitrary but due to it giving a good enough result it was kept. The filter then saved the indices of where the signal was above the threshold and then use the first and last indices as a start and stop for the observation. The observation was then expanded around the start and stop index to include more data. If there was a large enough gap in where the threshold was reached in one file it would count as two observations.

5.4 Testing the setup

As a way to test the software and setup a teflon ball was thrown into the probe volume to see if both the photodiodes and camera would react as well as to see if the times in both files would align. Due to the simplicity of the falling motion it could also be used to see if the 3D reconstruction was valid. Further testing was then done using live insects, fruit flies (*drosophila melanogaster*), that had been breed in a small test tube.

Chapter 6

Results of test chamber setup

6.1 Fruit fly (*drosophila melanogaster*)

As one can see in fig. 6.1a the strongest signal from the measurement is the co-polarized light from the 808 nm laser. The general shape of the co-polarized 808 signal is shared with the de-polarized 808 nm signal. The shape of the co- and de-polarized signal from the 1320 nm laser have a very different shape from the 808 nm signals which was to be expected. The 1320 nm signal also starts slightly after the 808 nm signal and doesn't even go back to zero within the figure. This is due to the two laser beams not being perfectly overlapping. The shape of the extinction signal is hard to interpret but can be seen to decreases as the fly enters the laser beam which is expected.

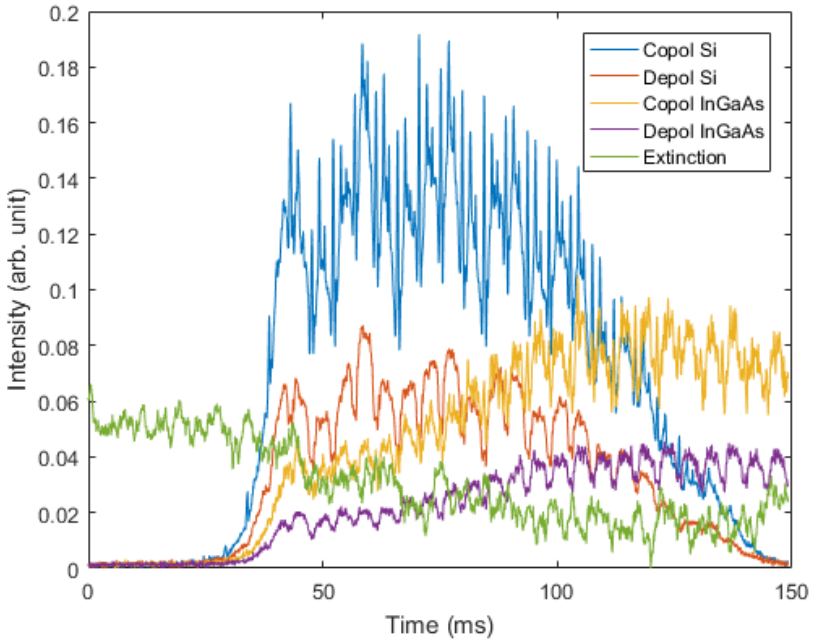

(a)

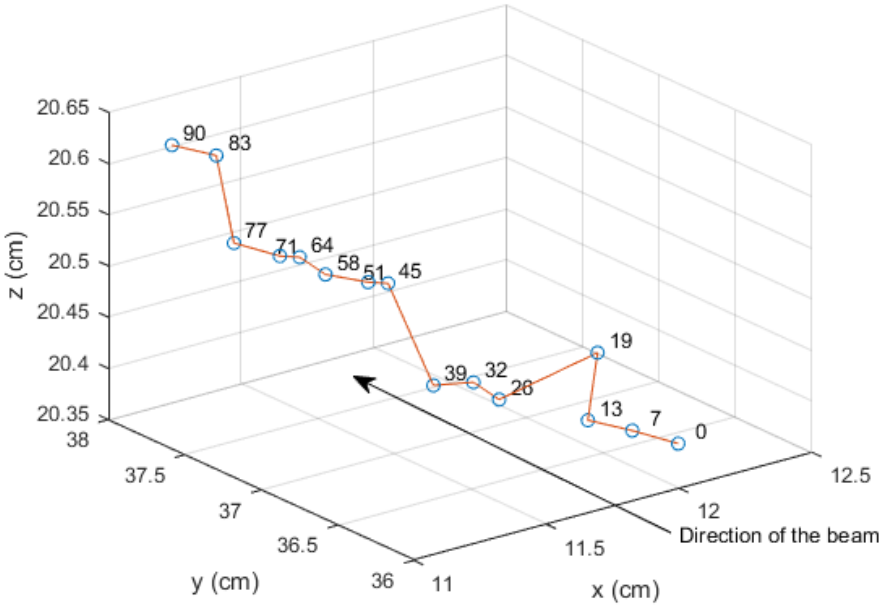

(b)

Figure 6.1: Measurement on a fruit fly together with the reconstructed flight path. Fig. 6.1a shows the recorded signals from a fruit fly where the minimum value from the different channels have been subtracted from the channel in order to more easily compare the signals. Fig. 6.1b shows the flight path of the same fruit fly with the time measured from the first taken image as numbers next to the data points. The arrow illustrate the direction of the laser beam

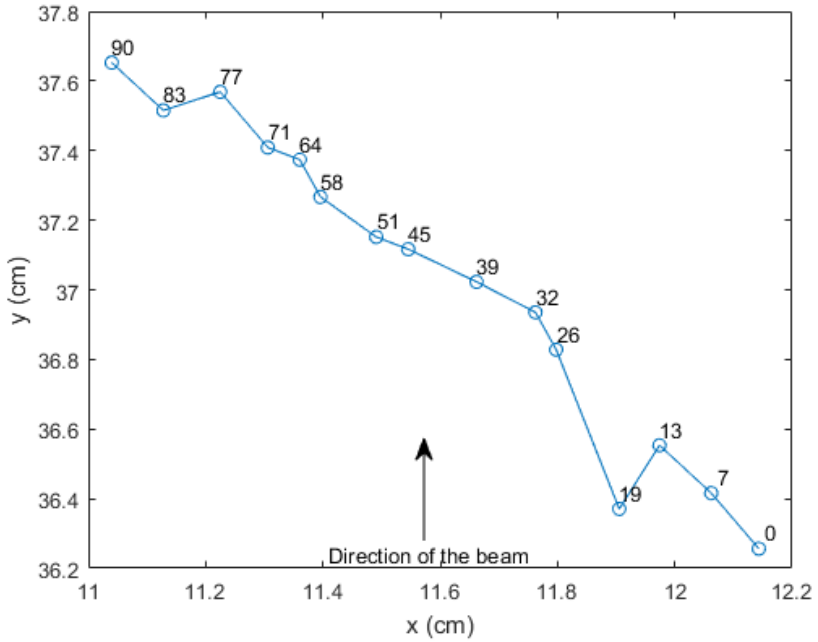

Figure 6.2: The flight path from fig. 6.1b shown in 2D for clarity's sake. The numbers next to the data points is the time when the image was taken.

In fig. 6.1b one can see that the average duration between the images were taken was around 6.4 ms which means that the full potential of the frame rate of the camera was utilised, since $\frac{1}{156} \approx 6.4$ ms

6.2 Time mismatch

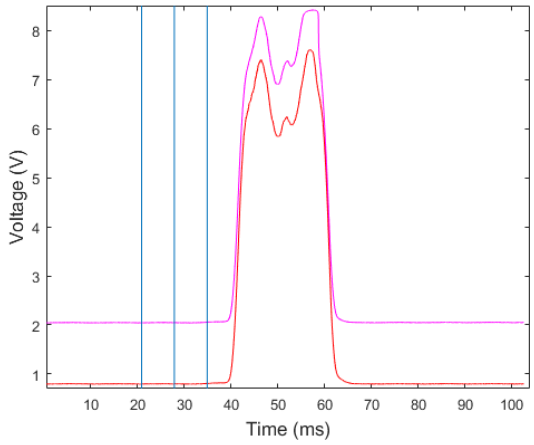

(a)

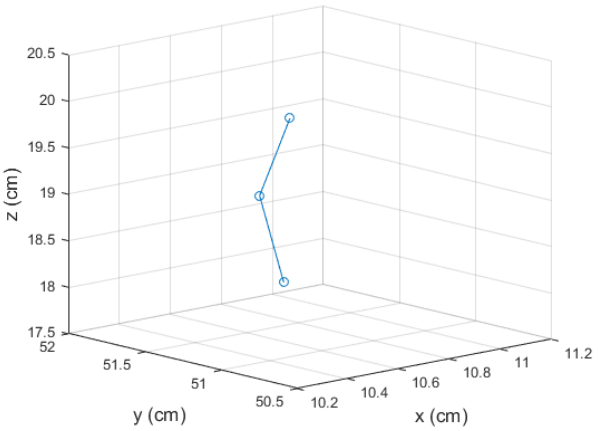

(b)

Figure 6.3: The recorded signal as well as the corresponding flight path of a dropped telfon ball with a diameter of 6 mm. Fig. 6.3a shows the signal from a teflon ball dropped into the probe volume with the copolarized Si detector signal in red, the depolarized in magenta and the time when the camera saved images marked in blue. Fig. 6.3b shows the flight path of the same teflon ball.

In fig. 6.3 one can see that there is a mismatch between when the camera and the photodiode signal. In fig. 6.3b one can see the reconstructed flight path of a dropped teflon ball. In fig. 6.4 one can see histograms of the estimated time mismatch. By comparing the two time differences in fig. 6.4a and fig. 6.4b the time mismatch that occurs between the data files and the camera files can be estimated. The mean value of fig. 6.4a was about 19 ms, even if one removes the two rather suspicious looking values at 0 and 61 one ends up with a mean value of 19 ms. The mean value of fig. 6.4b was about 25 ms removing the suspicious looking values in a similar fashion one ends up with the mean value of about 24 ms. Lastly fig. 6.5 is a histogram of the difference between the duration the observation based on the data file and the

duration between the first and last image taken.

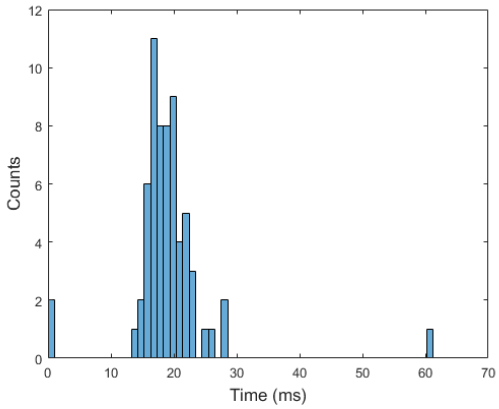

(a) Histogram over estimated time mismatch between the start of an observation and the first image taken

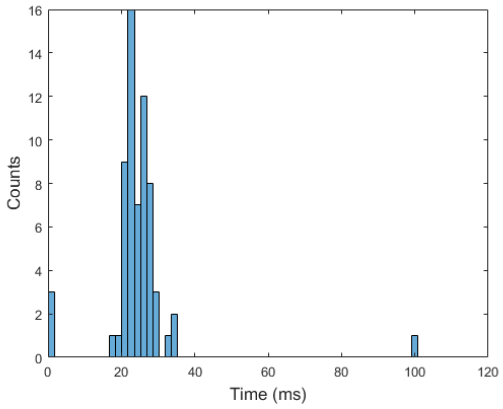

(b) Histogram over estimated time mismatch between the end of an observation and the last image taken

Figure 6.4: Histogram over estimated time mismatch

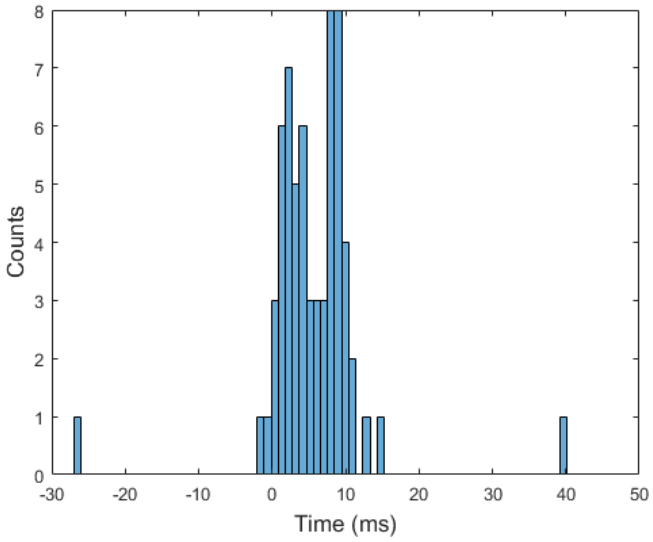

Figure 6.5: The time difference between the duration of an observation and the duration between the first image being taken and the last image of that observation

Chapter 7

Analysing real data obtained from test chamber setup

7.1 Analysis of real data

When the real data is obtained, the same procedure as with simulated data is done in order to produce phase estimations. This procedure corresponds to filtering out the body part of the signal, potentially applying denoising and shaping the data into Gaussian envelopes thereby also creating segments of the signal. After that, the segments will be analyzed by the matched reassignment and the matched phase reassignment, yielding phase estimations.

There are two big differences from the simulated data. The first one is that downsampling of a factor 4 will be done, using Matlab's function decimate, as described in the theory section. The second one is that the phases will no longer run between 0 and 0.5, but instead from 0 to 0.9. Using the interval $[0, 0.5]$ in the simulated data made sense since the actual phases could be controlled to be within that interval. However, for real data this cannot be controlled and it could be that the phases often lie above 0.5. It is still important to have the restriction of phases and not let the estimations run between $[0, 1]$, due to periodicity as explained previously. Therefore, the interval $[0, 0.9]$ was decided for real data, giving a margin of 0.1 before periodicity occurs, but still not limiting the phases too much.

The analysis of real data was first done on the fruit flies (*drosophila melanogaster*), taking out the fundamental frequency and two overtones. The sample size is the same as in the simulations, i.e. 100 samples.

7.2 Results from real data

7.2.1 Fruit flies (*drosophila melanogaster*)

The histograms for the estimated frequencies of the fruit flies are seen in fig. 7.1, fig. 7.2 and fig. 7.3, with the respective means and medians:

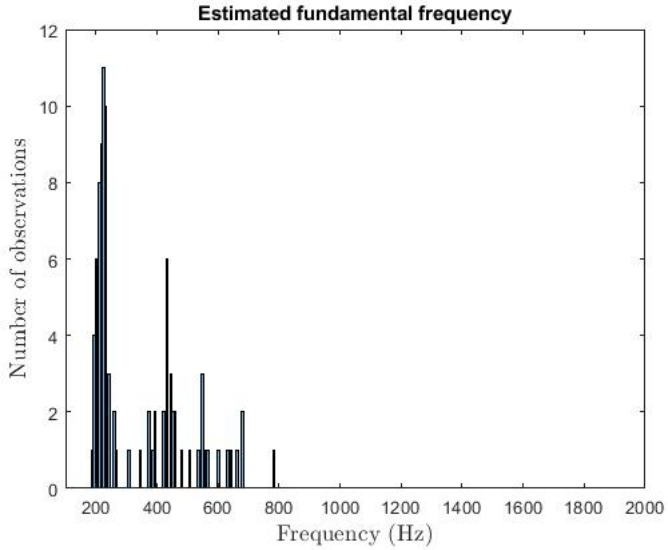

Figure 7.1: Histogram of estimated fundamental frequency.

The mean $\bar{x}$ and the median $\tilde{x}$ of the estimated fundamental frequency are

$$\begin{aligned} \bar{x} &= 329 \text{ Hz}, \\ \tilde{x} &= 232 \text{ Hz}. \end{aligned} \tag{7.1}$$

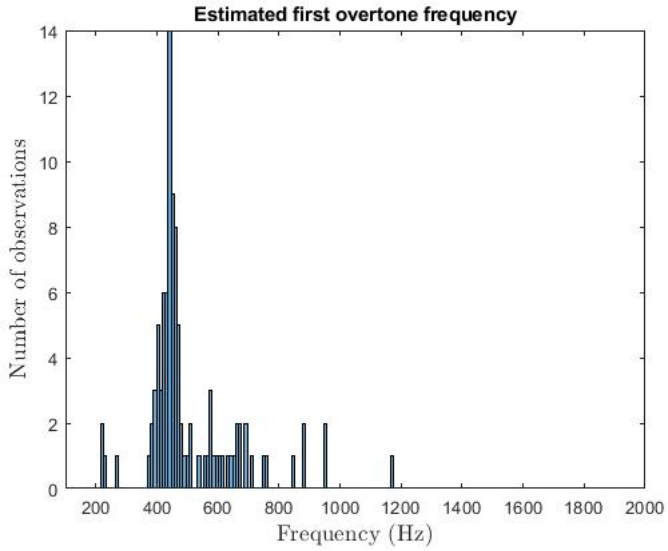

Figure 7.2: Histogram of estimated first overtone frequency.

The mean $\bar{x}$ and the median $\tilde{x}$ of the estimated frequency of the first overtone are

$$\begin{aligned} \bar{x} &= 505 \text{ Hz}, \\ \tilde{x} &= 452 \text{ Hz}. \end{aligned} \tag{7.2}$$

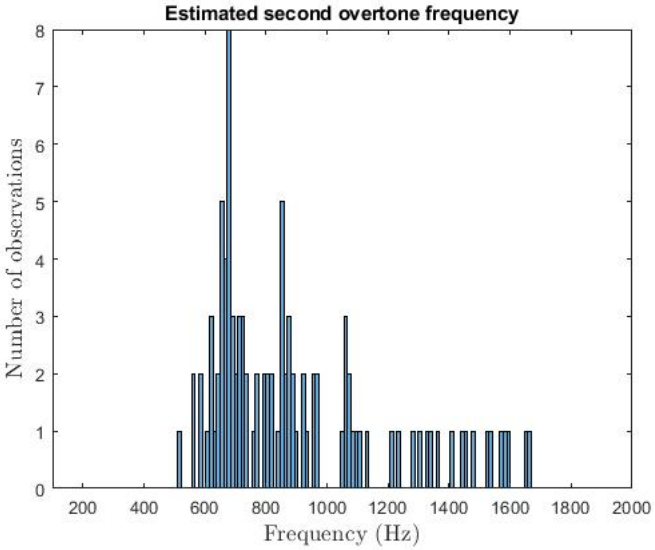

Figure 7.3: Histogram of estimated second overtone frequency.

The mean $\bar{x}$ and the median $\tilde{x}$ of the estimated frequency of the second overtone are

$$\begin{aligned} \bar{x} &= 905 \text{ Hz}, \\ \tilde{x} &= 819 \text{ Hz}. \end{aligned} \tag{7.3}$$

The analyzed real data was the fruit flies (*drosophila melanogaster*). This fly has a fundamental wing beat frequency of roughly 200 Hz. The estimations of the frequencies can be seen in the fig. 7.4, visualizing the spread of the estimations:

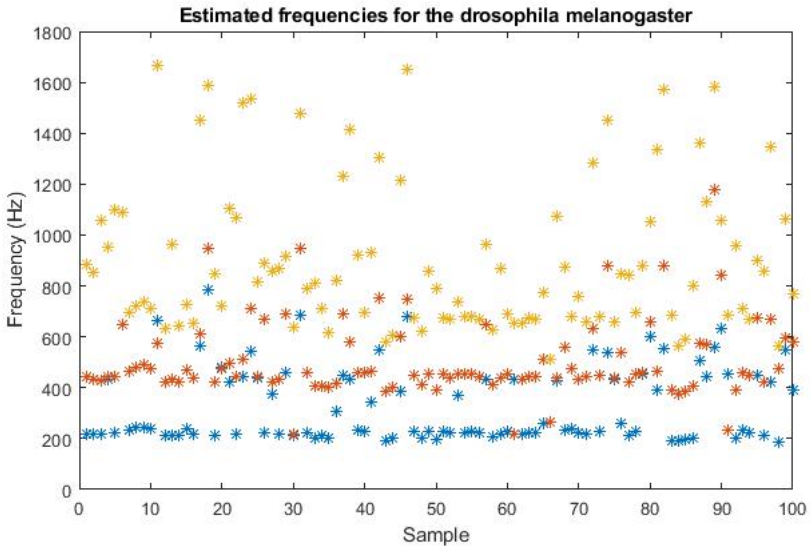

Figure 7.4: Estimated frequencies for the fruit flies (*drosophila melanogaster*).

As can be seen in fig. 7.4, the blue dots represents the estimation for the fundamental wing beat frequency, the red dots represents the estimation for the first overtone

and lastly the yellow represents the estimation for the second overtone. Here, the blue should correspond to roughly 200 Hz, the red to roughly 400 Hz and the yellow to 600 Hz. The spread of the yellow dots is a strong indication of that the estimated phase difference between the first and second overtone is not correctly estimated since the frequencies themselves are incorrectly classified.

The result for the phase difference between fundamental frequency and its first overtone can be seen in fig. 7.5

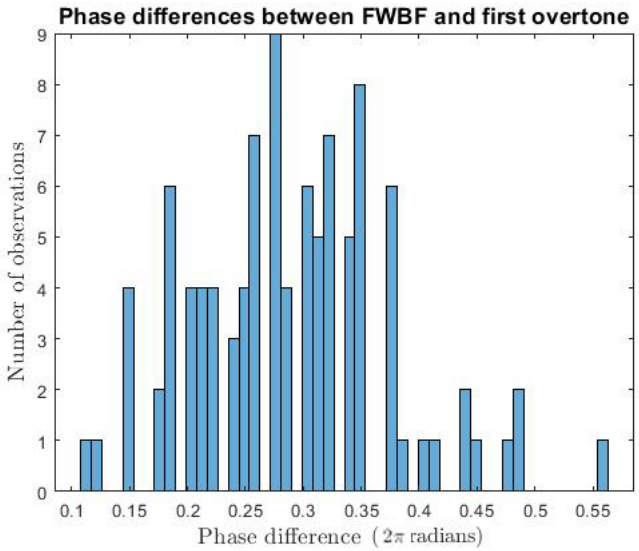

Figure 7.5: Histogram of phase difference between fundamental frequency and its first overtone.

The confidence interval, defined as,

$$\bar{x} \pm z\frac{\sigma}{\sqrt{n}}, \tag{7.4}$$

will be used. In the equation above, $\bar{x}$ is the mean of the data, z is the chosen z-value, i.e. corresponding confidence level, σ being the standard deviation and n the sample size. With a 95% confidence level, the results are as follows:

$$0.2895 \pm 0.0166 = \{0.27, 0.31\}. \tag{7.5}$$

For the phase difference between the first overtone and the second, the histogram is presented:

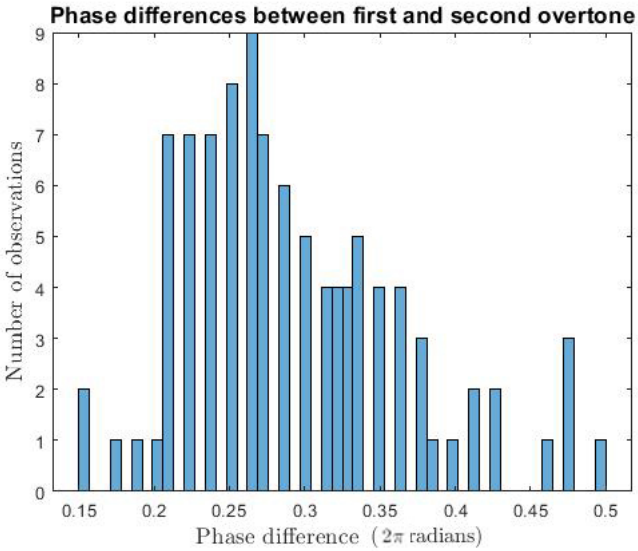

Figure 7.6: Histogram of phase difference between first and second overtone.

The confidence interval, with same confidence level, was calculated for these results as well:

$$0.2946 \pm 0.0143 = \{0.28, 0.31\}. \tag{7.6}$$

As can be seen in the two histograms, fig. 7.5 and fig. 7.6, and confidence levels above, the results for the phase difference between the fundamental frequency and its overtone, and the first and second overtone, are similar.

7.2.2 Yellow fever mosquitoes (*aedes aegypti*)

The same analysis was also started on the yellow fever mosquito (*aedes aegypti).* This data did not come from this thesis' test chamber setup, but was provided by Samuel Jansson (Department of Physics, Lund Laser Centre, Lund University, Lund, Sweden). This setup used 1550 nm laser instead of 1320 nm for the SWIR. This data was also analyzed in order to possibly get a difference in phases between the different species. Before running 100 simulations, the first ten was to be analyzed. The reason for this was that the simulations on a FWBF of 900 Hz pointed towards a strong misclassification of phases. The results of the frequency estimations of the first ten runs can be seen in fig. 7.7:

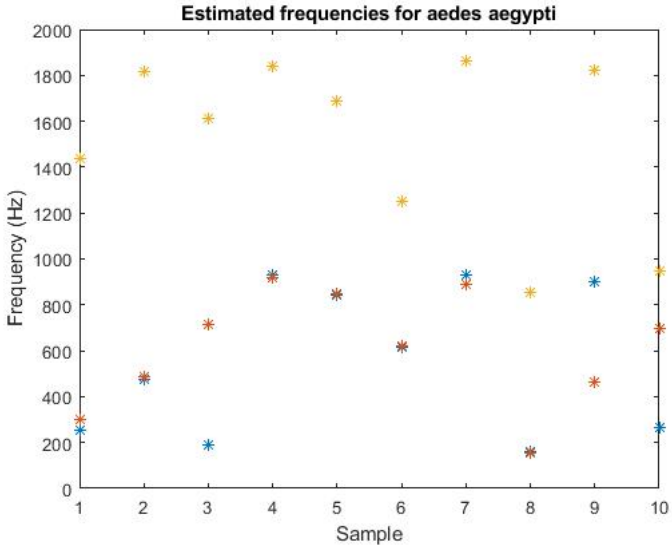

Figure 7.7: Estimated frequencies for the yellow fever mosquito (*aedes aegypti*) where blue is the FWBF, red is the first overtone and yellow is the second.

An example of the frequency estimation can be seen in the fig. 7.8:

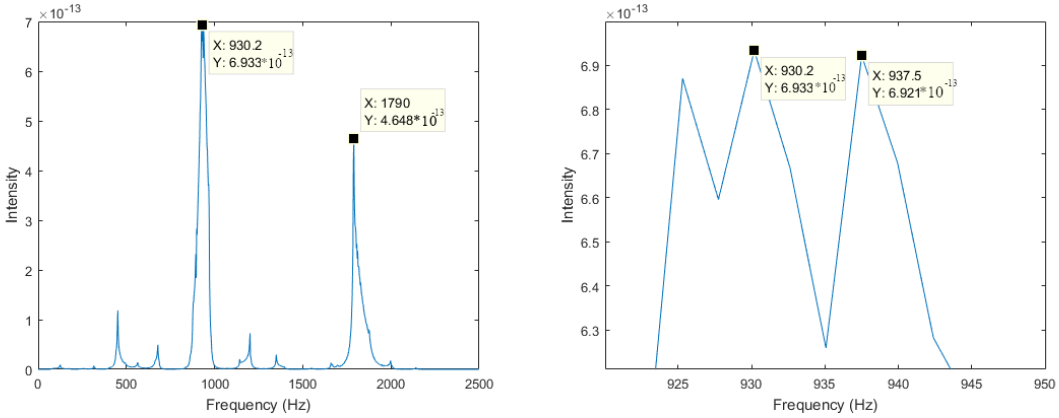

(a) (b)

Figure 7.8: Estimated frequencies for the yellow fever mosquito (*aedes aegypti*). An example of the spectrum from a yellow fever mosquito observation with what seems to be two obvious peaks in fig. 7.8a. The same spectrum but zoomed in fig. 7.8b on what seemed to be one peak in fig. 7.8a.

In fig. 7.8a one can see the two peaks the method should detect i.e the peaks at 930 and 1790 Hz, however the method instead returns two frequencies that are very close to each other. In fig. 7.8b one can see the same figure but zoomed in on the frequencies that the method returns instead. It is clear that the frequencies have been wrongly estimated. The yellow fever mosquito has a FWBF of roughly 900 Hz, which means that the overtones are around 1800 and 2700 Hz.

Due to the frequencies being wrongly estimated, the phases will be incorrectly esti-

mated as well. This is a logical implication, since a phase estimation of a frequency that does not correspond to the fundamental frequency or an overtone is not an interesting number, and thereby a misclassification.

The frequency estimations for the yellow fever mosquito had a large spread with randomness. In order to try to combat this, it was decided to use one large window per signal instead of 20 small ones to see if it would reduce the spread of frequencies estimated. This also reduced the run time, enabling 3700 runs to be made. Due to the strange shape of the mosquito observations, the observation could for example start long before any wing beats could be detected, it was decided to first attempt to filter out the body and then try to place the window on top of the maximum value. In order to avoid scenarios as portrayed in fig. 7.8 a minimum distance of 10 samples, corresponding to a frequency distance of about 24 Hz, was chosen.

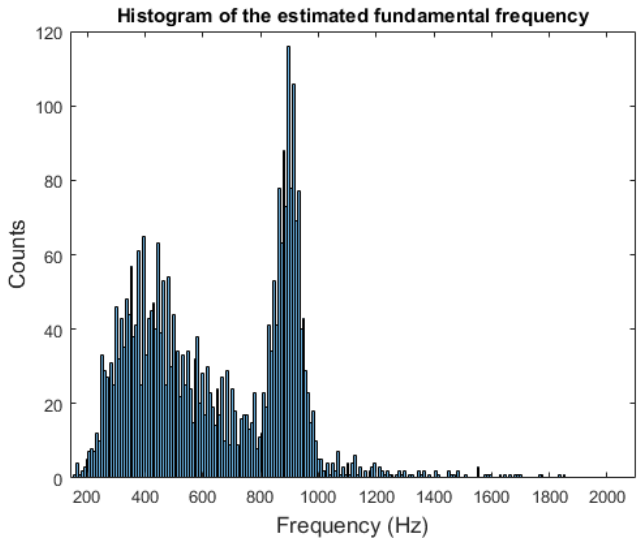

Figure 7.9: Estimated fundamental frequencies for the yellow fever mosquito (*aedes aegypti*) from 3700 runs.

In fig. 7.9, the estimated FWBF can be seen, from male yellow fever mosquitoes based on the signal from the co-polarized 1550 nm laser. The mean $\bar{x}$ and the median $\tilde{x}$ of the estimated fundamental frequency are

$$\begin{aligned} \bar{x} &= 644 \text{ Hz}, \\ \tilde{x} &= 615 \text{ Hz}. \end{aligned} \tag{7.7}$$

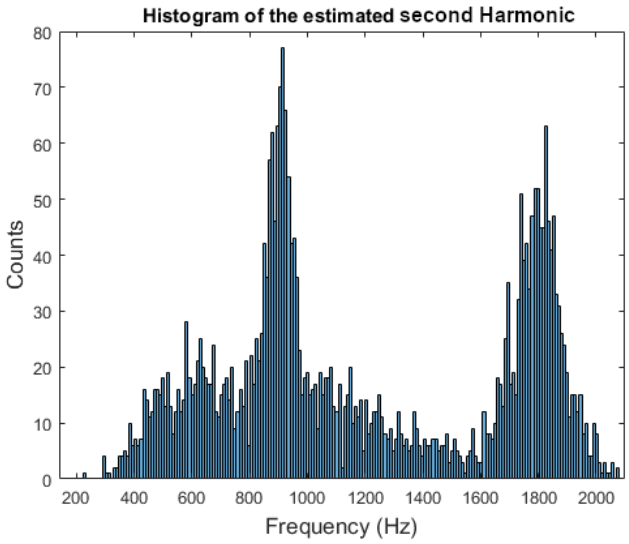

Figure 7.10: Estimated second harmonic frequencies for the yellow fever mosquito (*aedes aegypti*) from 3700 runs.

In fig. 7.10, the estimated first overtone with the overtone's mean and median are

$$\begin{aligned} \bar{x} &= 1200 \text{ Hz}, \\ \tilde{x} &= 1045 \text{ Hz}. \end{aligned} \tag{7.8}$$

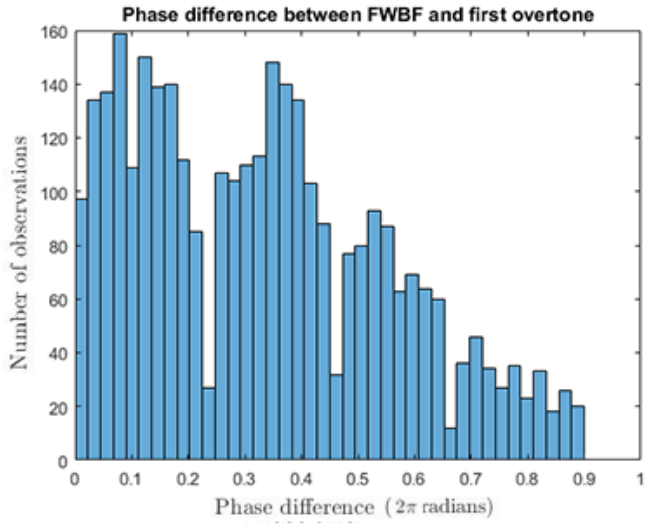

Figure 7.11: Histogram of phase difference between fundamental frequency and its first overtone.

This approach did not increase the accuracy of the results. The mean of the phase difference is 0.3343 and the confidence interval at 95% is

$$\{0.33, 0.34\} \tag{7.9}$$

Comparing fig. 7.11 and 7.14 suggests that the phase difference between the FWBF and first overtone can't be used as a distinguishing feature.

7.2.3 Southern house mosquitoes (*culex quinquefasciatus*)

The same procedure as with the yellow fever mosquito was done on the southern house mosquito (*culex quinquefasciatus*). The results are attached in fig. 7.12, fig. 7.13 and fig. 7.14.

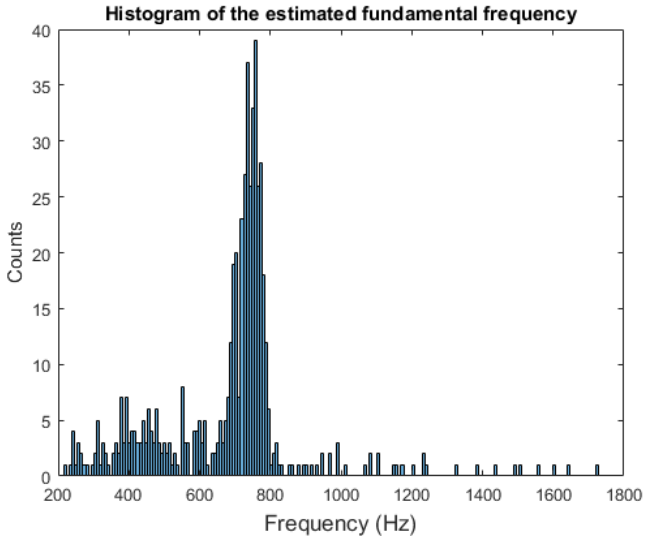

Figure 7.12: Estimated fundamental frequencies for the southern house mosquitoes from 554 runs.

The mean $\bar{x}$ and the median $\tilde{x}$ of the estimated fundamental frequency are

$$\begin{aligned} \bar{x} &= 686 \text{ Hz}, \\ \tilde{x} &= 728 \text{ Hz}. \end{aligned} \tag{7.10}$$

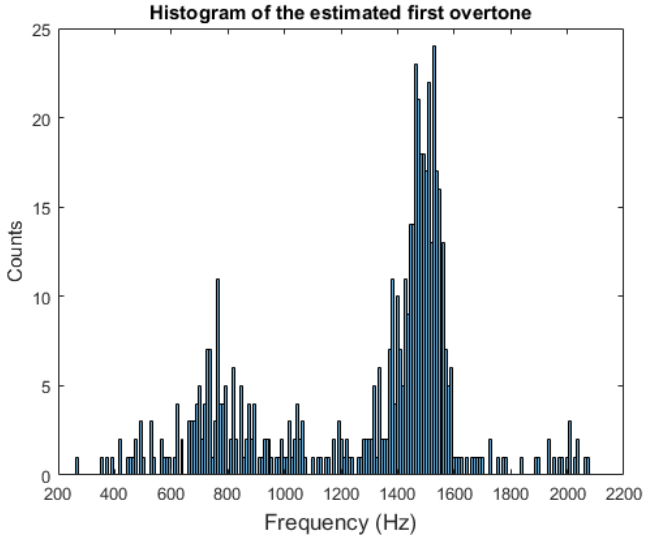

Figure 7.13: Estimated first overtone frequencies for the southern house mosquito from 554 runs.

The mean $\bar{x}$ and the median $\tilde{x}$ of the estimated fundamental frequency are

$$\begin{aligned} \bar{x} &= 1287 \text{ Hz}, \\ \tilde{x} &= 1450 \text{ Hz}. \end{aligned} \tag{7.11}$$

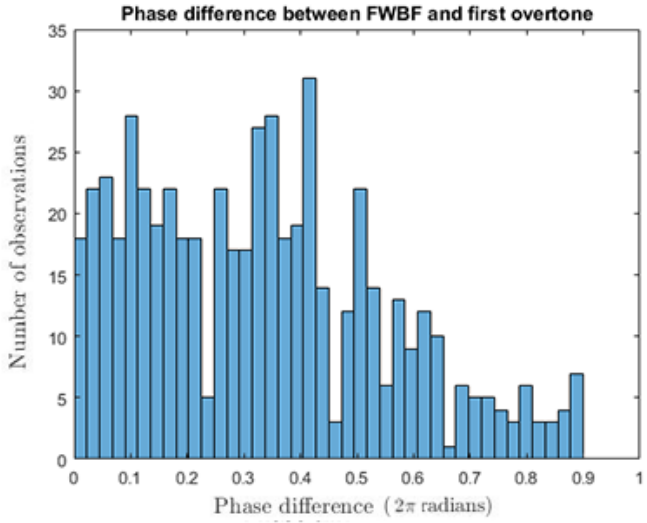

Figure 7.14: Histogram of phase difference between fundamental frequency and its first overtone.

The confidence interval with a 95% confidence level based on the data in fig. 7.14 yields:

$$\{0.31, 0.35\} \tag{7.12}$$

with a mean of 0.3324

Chapter 8

Discussion and Conclusion

8.1 Matched Phase Reassignment

The matched phase reassignment method is sensitive to noise. Although sensitive to noise, the simulated signals' phase estimation performed quite well even though large amount of noise was added. For an SNR level of 10, the first phase difference had an average error of 0.07 which was lower than expected. For signals with higher levels of SNR, the error decreases which also was expected, and the algorithm performs very well for SNR levels $15 - 20$, which were satisfying results. This level of noise corresponds well to the amount of noise that was present in real data which points towards that if the recorded data have a reasonable amount of noise the algorithm can perform to a satisfying degree, depending on purpose. Furthermore, the final simulations were made on a fundamental wing beat frequency of 200 Hz. 100 simulations were made on each parameter, taking roughly 12 hours to perform for each parameter. From the initial assessment it was quite clear that the results would be poor for higher FWBF's, which was the reason for why 200 Hz was focused on. Furthermore, 100 simulations were made on a FWBF of 900 Hz which confirmed the suspicions of poor performance in higher FWBFs. It would have been interesting to have some more statistically robust results on higher FWBFs, and at what frequencies the algorithm starts to fail. From a time perspective it was important to narrow down the space of parameters by doing the initial assessment with lower amounts of simulations.

One reason for why the phases are wrongly estimated is due to the frequencies being estimated with errors. Since the matched phase reassignment method relies on the frequencies of the signal correctly being estimated, this heavily affect the end outcome. Implementing ways of "intervening" between the frequency estimation and the matched phase reassignment and there potentially correcting or discarding certain frequency estimations could be a way to partially fix this. The problem with this is that for real data, no prior information about frequencies exists and therefore it would be hard to classify wrongly and correctly estimated frequencies. There could potentially be information about species-specific properties, but even if these frequencies deviate with a few percent due to for example high levels or noise corrupts the end results. This thesis had the approach to create the best circum-

stances for the algorithms to work well with the data at hand, and then evaluating the results. The reason behind this was to assess and quantify the performance of the phase estimation, with the best possible circumstances, instead of intervening and "improving" the results, thereby creating results that perhaps would not be obtainable without same adjustments, thus not representing a correct image of the performance.

8.1.1 Future work on this topic

As explained in the previous section, a large source of error was the wrong classification of frequencies. Previous work has been done on frequency estimations, but the importance of correctly classifying the frequencies in order for the phase estimation to work cannot be emphasized enough. Therefore, it would be interesting to see case-specific frequency estimations, exploring what actions that can be taken in order to improve the frequency estimation on insects in particular.

Furthermore, it was clear that the data obtained through real experiments contained noise and that the phase estimations were affected by this. This was also confirmed in the simulations. An attempt to denoise the data was made using wavelets. Denoising is a tricky and time-consuming subject to cover which led to after implementing wavelets with thresholding this area was deemed to be sufficient for the purposes of this thesis. The scope of this thesis was not to implement a denoising technique, but was added as a way of hopefully improving the results since the matched phase reassignment method was known to be sensitive to noise. It was clear from the results on simulated data that the denoising technique implemented in this thesis was not sufficient to drastically improve the accuracy. It would be interesting to see further work on how denoising techniques could help the algorithms perform better, rather than having this topic as a peripheral.

Lastly, one big restriction placed on the model was the restriction of phases in the simulations. In order to combat the problem of the periodicity in phases and that the results become skewed, the restriction of letting the phases run between 0 and $\frac{1}{2}$ was implemented. As stated, this reduces the space of where the model is applicable. Developing an algorithm or model for combating this problem would be highly interesting in further work in this subject.

8.2 Test chamber setup

A problem that consistently came up for the setup was the time mismatch between the signal from the photodiodes and the camera which makes it hard to match them with each other. Fortunately the mismatch seemed to be relatively consistent with the delay of about 20 ms. With enough images taken during an observation to cover the entire flight through the laser beam, for example fig. 6.3a, one could probably overlap the signal and images with decent certainty. There was also a problem with when the matrices from the camera are saved some images are lost due to the processing time exceeding the time between images but since the saving only was done

when no insect was in the camera's field of view it had a marginal effect.

There was also a thought that the phase difference between the FWBF and the first overtone could potentially reveal some information about the heading of the insect since using the phase difference as a way to distinguish different insects seemed somewhat futile. This however, failed and no correlation between the phase and heading could be determined.

8.2.1 Future work on this topic

Further improvements to the setup could be done by figuring out a better way to utilise the extinction signal which goes completely unused as is. Another problem can arise if two insects are within the field of view at the same time. Currently the software for the camera will only save the location of one of the insects and that is if either of the insects are within the cameras field of view.

Appendices

Appendix A

A.1 Initial simulations performed prior to the 100 simulations

In this section of the appendix, the numbers from the initial test simulations are presented in a table format. This is for the reader to take a closer look if interested in the hard numbers which led to the conclusions presented in the simulation section regarding settings to use for further simulations.

These results were presented in a figure, previously in the report, as well.

A.1.1 Notation

The following notation is used in the tables:

FWBF – Fundamental wing beat frequency,
Fs – Sampling frequency,
K – Number of tones (including fundamental wing beat frequency, i.e. $K = 1$ represents just the fundamental wing beat frequency),
SNR – Added noise level expressed as SNR,
Run – Simulation number,
T12 – True phase difference between tone 1 and 2,
A12 – Approximated phase difference between tone 1 and 2.

The settings are seen in the left table, and the results in the right.

A.1.2 Initial simulations

FWBF	200
Fs	1000
K	2
SNR	0

Run	1	2	3	4	5
T12	0.1	0.1	0.3	0.2	0.2
A12	0.1	0.1	0.3	0.2	0.2

FWBF	200
Fs	1000
K	3
SNR	0

Run	1	2	3	4	5
T12	0.1	0.2	0.1	0	0.2
T23	0.2	0	0.2	0.1	0.1
A12	0.2	0.1	0.1	0.1	0.5
A23	0.2	0.4	0.1	0	0.4

FWBF	200
Fs	1000
K	4
SNR	0

Run	1	2	3	4	5
T12	0.2	0.3	0.2	0.4	0.2
T23	0.2	0.2	0	0.2	0.2
T34	0.1	0.1	0	0.1	0.2
A12	0.1	0.2	0.2	0	0.1
A23	0.4	0.1	0	0.1	0.1
A34	0.1	0.4	0.1	0.5	0.5

FWBF	200
Fs	2500
K	3
SNR	0

Run	1	2	3	4	5
T12	0.1	0.2	0	0.2	0
T23	0.1	0	0	0.2	0
A12	0.2	0.3	0.1	0.1	0.1
A23	0.1	0	0	0.2	0

FWBF	200
Fs	2500
K	4
SNR	0

Run	1	2	3	4	5
T12	0.2	0.1	0	0.2	0
T23	0.2	0.1	0.1	0.2	0.2
T34	0.1	0.4	0.1	0.1	0.1
A12	0.3	0	0.1	0.2	0.1
A23	0.2	0	0.1	0.1	0.1
A34	0.2	0.5	0.3	0.3	0.2

FWBF	200
Fs	5000
K	4
SNR	0

Run	1	2	3	4	5
T12	0.1	0.2	0.1	0.1	0.1
T23	0	0.2	0.1	0.1	0.1
T34	0.1	0.4	0.1	0	0.2
A12	0.1	0.2	0.1	0	0
A23	0	0.2	0.1	0.1	0
A34	0.1	0.3	0.1	0	0.05

FWBF	200
Fs	5000
K	5
SNR	0

Run	1	2	3	4	5
T12	0.3	0.1	0.4	0.2	0.1
T23	0	0.1	0.1	0.1	0.3
T34	0	0.2	0.2	0.3	0.1
T45	0.1	0.4	0	0.2	0.1
A12	0.2	0.1	0.4	0.2	0.1
A23	0	0.1	0.1	0	0.3
A34	0	0.2	0.2	0.2	0.1
A45	0.1	0.3	0	0.2	0.1

FWBF	500
Fs	5000
K	3
SNR	0

Run	1	2	3	4	5
T12	0.1	0.2	0.3	0.4	0.2
T23	0.4	0	0.1	0.1	0.3
A12	0	0.1	0.3	0.2	0.2
A23	0.2	0.2	0.4	0.2	0.5

FWBF	500
Fs	5000
K	4
SNR	0

Run	1	2	3	4	5
T12	0.1	0.3	0	0.3	0
T23	0.1	0.1	0.2	0.3	0
T34	0.3	0	0	0.2	0.3
A12	0.2	0.3	0.1	0.2	0
A23	0.3	0.4	0.2	0.1	0.3
A34	0.1	0.1	0.1	0.1	0.2

FWBF	900
Fs	10000
K	3
SNR	0

Run	1	2	3	4	5
T12	0.2	0.5	0	0.4	0.2
T23	0.1	0.2	0.4	0	0.3
A12	0.1	0.5	0.2	0.5	0.5
A23	0.4	03	0.05	0.25	0.25

FWBF	900
Fs	10000
K	4
SNR	0

Run	1	2	3	4	5
T12	0.1	0	0.2	0.2	0
T23	0.1	0	0.1	0.1	0.1
T34	0.1	0.1	0.1	0	0
A12	0.1	0.3	0.4	0.5	0.1
A23	0.3	0.2	0.2	0.25	0.25
A34	0.2	0.3	0.2	0.3	0.3

FWBF	200
Fs	5000
K	3
SNR	40

Run	1	2	3	4	5
T12	0.3	0.2	0.3	0.4	0.3
T23	0.1	0.1	0.3	0.4	0.2
A12	0.3	0.2	0.3	0.3	0.3
A23	0.1	0.05	0.3	0.3	0.2

FWBF	200
Fs	5000
K	3
SNR	30

Run	1	2	3	4	5
T12	0	0	0.1	0.3	0
T23	0.4	0.1	0.2	0.1	0.3
A12	0	0.05	0.1	0.3	0
A23	0.3	0.1	0.2	0	0.3

FWBF	200
Fs	5000
K	3
SNR	20

Run	1	2	3	4	5
T12	0.2	0	0.3	0.1	0.1
T23	0.1	0.5	0.2	0.2	0.1
A12	0.2	0	0.2	0	0.1
A23	0.1	0.4	0.2	0.2	0.1

FWBF	200
Fs	5000
K	3
SNR	10

Run	1	2	3	4	5
T12	0.1	0.1	0	0.1	0.1
T23	0.4	0.1	0.1	0	0.2
A12	0.15	0.2	0.1	0.25	0.2
A23	0.2	0.2	0.3	0.1	0.3

FWBF	200
Fs	5000
K	3
SNR	10
Denoised	Yes

Run	1	2	3	4	5
T12	0.2	0.4	0.1	0.1	0.1
T23	0.2	0.4	0.1	0.4	0.1
A12	0.1	0.3	0.15	0.15	0.2
A23	0.2	0.3	0.3	0.3	0.2

A.2 Populärvetenskaplig beskrivning

Insekter är en essentiell komponent i många ekosystem. Rollerna som de har är viktiga, vilka inkluderar spridning av växters frön, pollinering och att vara en källa till näring för andra djur. Dock finns aspekter med insekter som innebär hot för människor. Exempelvis kräver malaria cirka 400 000 människoliv per år, en sjukdom som förs vidare av myggor.

För att kunna bekämpa sjukdomar som malaria är det viktigt att få djupare förståelse och kunskap om dessa djur. Ett led i detta är att på ett korrekt sätt kunna klassificera dem, vilket tidigare har gjorts genom att exempelvis titta på vilken frekvens respektive insektsart slår med sina vingar. Som exempel har de vanliga bananflugorna en vingslagsfrekvens på cirka 200 slag i sekunden, medan en gulafebernmygga har en vingslagsfrekvens på cirka 900 slag i sekunden. Ett problem med denna metod är att det finns ett väldigt stort antal olika arter av insekter som är intressanta att analysera, vilket i sin tur gör att det är svårt att få en unik vingslagsfrekvens för varje specifik art.

I denna uppsats har de relativa faserna mellan insekters övertoner studerats, med motivering att det möjligen finns artspecifika egenskaper i faserna som kan hjälpa till med klassificering. Detta har gjorts med en nyligen utvecklad metod kallad *matched phase reassignment*. Denna metod hittar graden av synkronisering mellan två olika signaler och på så sätt skattas faserna för dessa. Algoritmen kan appliceras på enskilda signaler, i detta fall insektsdata, genom att estimera frekvenserna för insekten och sedan skapa surrogatdata med samma frekvens. Dessa två signaler är således helt synkroniserade när faserna överensstämmer, vilket i sin tur ger en fasestimering.

Resultaten visar på att metoden för att estimera faser är känslig för vilken typ av signal det är. I vissa fall fungerar det mycket väl (exempelvis för relativt låg nivå av brus samt en låg vingslagsfrekvens), medan i andra fall sämre. Som tidigare nämnts baseras fasestimeringen på synkroniseringen mellan två signaler. För att två signaler ska kunna vara synkroniserade är det en förutsättning att frekvenserna är samma. Det är alltså mycket viktigt att frekvensskattningen av insekterna blir bra, eftersom denna direkt påverkar skattningen av faser. I denna uppsats användes metoden *matched reassignment* för att skatta frekvenserna hos insekter. Det var tydligt att för högre vingslagsfrekvenser var frekvensskattningen inte lika bra som för lägre, vilket innebär att fasestimeringen påverkas i stor utsträckning.

För att kunna titta på riktig data byggdes en experimentell uppställning. I denna användes olika typer av laser för att spela in data av levande insekter som sedan kunde analyseras. Denna uppställning fungerade mycket väl och kommer att kunna användas i framtiden för samma ändamål. Detta är således ett verktyg som möjliggör kontinuerlig analys av insekter och som kan vara ett steg i att få mer förståelse för dessa djur.

Bibliography

[1] P.H. Adler. R.G. Foottit. *Insect Biodiversity: Science and Society, Volume II*. John Wiley & Sons Ltd., 2018.

[2] World Health Organization. *Vector-borne diseases*. 2017. URL: https://www.who.int/news-room/fact-sheets/detail/vector-borne-diseases (visited on 01/03/2020).

[3] S. Jansson et al. "First Polarimetric Investigation of Malaria Mosquitos as Lidar Targets". eng. In: IEEE Journal of Selected Topics in Quantum Electronics 25.1 (2019), pp. 1–8. ISSN: 0792-1233. DOI: 10.1109/JSTQE.2018.2859225. URL: http://dx.doi.org/10.1109/JSTQE.2018.2859225.

[4] A. Gebru et al. "Multiband modulation spectroscopy for the determination of sex and species of mosquitoes in flight". English. In: *Journal of Biophotonics* 11.8 (2018). ISSN: 1864-063X. DOI: 10.1002/jbio.201800014.

[5] M. Sandsten, R. Anderson, I. Reinhold and J. Brynolfsson. *The Matched Reassigned Cross-Spectrogram for Phase estimation*. Proc. of ICASSP. 2020.

[6] M. Brydegaard, A. Gebru, and S. Svanberg. "Super Resolution Laser Radar with Blinking Atmospheric Particles - Application to Interacting Flying Insects". English. In: *Progress in Electromagnetics Research* 147 (2014), pp. 141–151. ISSN: 1070-4698. DOI: 10.2528/PIER14101001.

[7] M. Brydegaard et al. "The Scheimpflug lidar method". eng. In: *Lidar Remote Sensing for Environmental Monitoring 2017*. Vol. 10406. SPIE, 2017. ISBN: 9781510612693. DOI: 10.1117/12.2272939. URL: http://dx.doi.org/10.1117/12.2272939.

[8] S. Jansson et al. "Correlation of mosquito wing-beat harmonics to aid in species classification and flight heading assessment". English. In: *Novel Biophotonics Techniques and Applications V*. Ed. by Arjen Amelink and Seemantini K. Nadkarni. Vol. 11075. Progress in Biomedical Optics and Imaging - Proceedings of SPIE 60. United States: SPIE, Oct. 2019. DOI: 10.1117/12.2527224.

[9] M. Brydegaard. "Towards Quantitative Optical Cross Sections in Entomological Laser Radar – Potential of Temporal and Spherical Parameterizations for Identifying Atmospheric Fauna". In: *PLoS ONE* 10 (Aug. 2015). DOI: 10.1371/journal.pone.0135231.

[10] M. Sandsten. *Time-Frequency Analysis of Time-Varying Signals and Non-Stationary Processes: An Introduction*. http://www.maths.lu.se/fileadmin/maths/personal_staff/mariasandsten/TFkompver2.pdf. 2018.

[11] J.O. Smith et al. *Spectral Audio Signal Processing*. W3K, 2011. ISBN: 9780974560731. URL: https://ccrma.stanford.edu/~jos/sasp/.

[12] J. Fogelmark. *Unbiased pitch detection and phase estimation in entomological lidar*. eng. Master Thesis. 2019.

[13] P. Laguna L. Sörnmo. *Bioelectrical Signal Processing in Cardiac and Neurological Applications*. Academic Press, 2005. ISBN: 978-0-12-437552-9.

[14] The MathWorks Inc. L. Shure. *Decimation — decrease sample rate by integer factor*. URL: https://se.mathworks.com/help/signal/ref/decimate.html (visited on).

[15] C. Lee B. Song. "Toward a Mechanistic Understanding of Color Vision in Insects". In: *Annalen der Physik* 322.10 (1905), pp. 891–921. DOI: http://dx.doi.org/10.1002/andp.19053221004.